# Toward extracting the scattering phase shift from integrated correlation functions. II. A relativistic lattice field theory model

Peng Guo®\*

College of Arts and Sciences, Dakota State University, Madison, South Dakota 57042, USA and Kavli Institute for Theoretical Physics, University of California, Santa Barbara, California 93106, USA

(Received 26 February 2024; accepted 10 June 2024; published 9 July 2024)

In the present work, a relativistic relation that connects the difference of interacting and noninteracting integrated two-particle correlation functions in finite volume to infinite volume scattering phase shift through an integral is derived. We show that the difference of integrated finite volume correlation functions converges rapidly to its infinite volume limit as the size of the periodic box is increased. The fast convergence of our proposed formalism is illustrated by analytic solutions of a contact interaction model, the perturbation theory calculation, and also the Monte Carlo simulation of a complex  $\phi^4$  lattice field theory model.

#### DOI: 10.1103/PhysRevD.110.014504

#### I. INTRODUCTION

Few nucleon interactions provide crucial inputs to nuclear many-body studies of matter: such as the neutron-star equation of state and stability of neutron-rich isotopes [1], exotic decays of various nuclei [2], and experimental searches for new physics beyond-Standard-Model particles [3]. The fundamental theory of nuclear physics is quantum chromodynamics (QCD), the theory of the strong interaction between quarks mediated by gluons. The only model-independent and systematically improvable method for computing the properties and interactions of nucleons directly from QCD is lattice QCD (LQCD), which is the Euclidean spacetime formulation of QCD on a finite and discrete lattice in a periodic hypercubic box. As the consequence of calculation in Euclidean spacetime and in a finite box, the energy spectra become discrete, no asymptotic states and no direct access to scattering amplitudes are available, and finite volume effect must be taken into account.

To map out nucleon-nucleon scattering amplitudes in the LQCD calculation, the Lüscher formula [4] has been widely used, which relates discrete energy levels of finite volume systems to their scattering phase shifts in a compact form. The typical two-step procedure follows: (1) first, extracting the low-lying energy spectrum by fitting

Published by the American Physical Society under the terms of the Creative Commons Attribution 4.0 International license. Further distribution of this work must maintain attribution to the author(s) and the published article's title, journal citation, and DOI. Funded by SCOAP<sup>3</sup>. exponential decaying behavior of correlation functions in Euclidean spacetime, and looking for the plateau in temporal correlation functions when Euclidean time is large enough so that the lowest energy level becomes dominant and correlation functions are free of excited states pollution; (2) the discrete energy spectra thus are converted into scattering phase shifts by applying the Lüscher formula. The two-step Lüscher formula approach has been proven to be very successful in the number of applications especially in the meson sector (see, e.g., Refs. [5–17]). The formalism has been quickly extended to include inelastic effects, such as a coupled-channel effect and three-body problems (see, e.g., Refs. [17–47]). Unfortunately the application of the two-step Lüscher formula approach in two-nucleon systems is hindered by a few challenges:

(i) The signal-to-noise ratio (S/N) [48,49] in stochastic evaluation of the path integral for the correlation of two-nucleon systems at large Euclidean times behaves as

$$\mathcal{R}(\tau) \overset{\tau \to \infty}{\sim} e^{-(m_N - \frac{3}{2}m_\pi)\tau},\tag{1}$$

where  $m_N$  and  $m_\pi$  are the nucleon and pion mass. Exponentially more statistics are required to overcome the S/N problem.

(ii) A large volume leads to a significant increase of density of states with small splitting between energy levels:  $\triangle E \approx \frac{1}{m_N} (\frac{2\pi}{L})^2$ , where L is a spatial extension of the lattice. The required Euclidean time  $\tau$  to display the signal of clear plateau must be  $\tau \gg (\triangle E)^{-1} \sim m_N (L/2\pi)^2$ , which could be well into the region where the noise has swamped the signal.

<sup>\*</sup>Contact author: peng.guo@dsu.edu

(iii) The difficulties of the Lüscher formula approach at a large volume limit increase significantly due to the increasingly dense finite volume spectrum and the large number of interpolating operators that are required to faithfully project out desired low-lying energy levels (see, e.g., Ref. [50]).

The challenges have prevented substantive progress on the calculation of two-nucleon interactions in LQCD. Even with all the technological advancements in computational science, there are still no calculations of two-nucleon systems utilizing the Lüscher formula with pion masses lighter than 300 MeV.

These challenges also motivate exploration of alternatives to the two-step Lüscher formula approach. The HAL QCD Collaboration potential method [51-55] was developed a decade ago and may offer an alternative approach to determining two-nucleon interactions at low energies without ground state saturation. Unfortunately, results from the two-step Lüscher formula method and HAL QCD Collaboration potential method do not agree, not even qualitatively at a very heavy pion mass [49]. The discrepancy between the Lüscher formula approach and the HAL QCD Collaboration potential method is known as the twonucleon controversy and poses a severe challenge to the LQCD prediction on few-nucleon dynamics. Some other new ideas have also been proposed in recent years, such as determining scattering amplitudes from finite volume spectral functions in Ref. [50], extraction of spectral densities from lattice correlators in Refs. [56,57], and extracting phase shifts from integrated correlation functions [58].

In Ref. [58], we show that the difference of integrated finite volume two-particle correlation functions between the interacting and free nonrelativistic particles system to infinite volume is related to the scattering phase shift,  $\delta(\varepsilon)$ , through an integral weighted by a factor  $e^{-\varepsilon\tau}$ ,

$$C(t) - C_0(t) \mathop{\to}_{t=-i\tau}^{L\to\infty} \frac{\tau}{\pi} \int_0^\infty d\epsilon \delta(\epsilon) e^{-\epsilon\tau}, \tag{2}$$

where C(t) and  $C_0(t)$  are integrated correlation functions for two nonrelativistic interacting and noninteracting particles in the finite box, respectively. L stands for the size of the periodic box, and t and  $\tau$  are Minkowski and Euclidean time, respectively. Most importantly, we also demonstrated in Ref. [58] that the difference of integrated finite volume two-particle correlation functions rapidly approaches its infinite volume limit that is given by the right-hand side of Eq. (2) at short Euclidean time,  $\tau \ll L$ , even with a modest small size box. The fast convergence feature of Eq. (2) at short Euclidean time  $(\tau/L \ll 1)$  makes it potentially a good candidate to overcome the S/N problem in the two-nucleon LQCD calculation. The proposal of Ref. [58] in principle is free from issues, such as increasingly dense energy spectra at large volume and ground state saturation. Hence, it also offers a more suitable framework to overcome the

challenges that the conventional two-step Lüscher formula faces at the large volume limit.

The aim of the present work is to extend the non-relativistic formalism proposed in Ref. [58] to a relativistic one. After installing all the relativistic kinematic factors, we will show later on that the relativistic version of Eq. (2) in 1+1 dimensions is given by

$$\Delta C(t) \stackrel{t=-i\tau}{=} \sum_{n=0}^{\infty} \left[ \frac{e^{-E_n \tau}}{E_n} - \frac{e^{-E_n^{(0)} \tau}}{E_n^{(0)}} \right]$$

$$\stackrel{L \to \infty}{\underset{t=-i\tau}{\to}} \frac{1}{\pi} \int_{2m}^{\infty} d\epsilon \delta(\epsilon) \left( \tau + \frac{1}{\epsilon} \right) \frac{e^{-\epsilon \tau}}{\epsilon}, \tag{3}$$

where  $E_n$  and  $E_n^{(0)}$  are eigenenergies of interacting and noninteracting relativistic two-particle systems, respectively, and m stands for the mass of two identical particles. The fast convergence of  $\triangle C(t)$  into its infinite volume limit given by the relation in Eq. (3) will be illustrated by (1) an exactly solvable contact interaction model, (2) a perturbation theory calculation, and (3) a Monte Carlo simulation of a complex  $\phi^4$  lattice field theory model.

The paper is organized as follows. First of all, a field theory model for the study of relativistic spinless particles interaction is set up in Sec. II. The derivation of the infinite volume limit of the integrated two-particle correlation function, its relation to particle scattering phase shift, and exact solutions and perturbation calculation of contact interaction results are all presented in Sec. II. The two dimensional (one spatial and one temporal dimensions) Monte Carlo simulation test of the  $\phi^4$  field is presented and discussed in Sec. III. The discussions and summary are given in Sec. IV.

## II. A LATTICE FIELD THEORY MODEL

In the present work, we will consider a relativistic lattice field theory model for the interaction of charged scalar particles via a short-range potential in one spatial and one temporal dimensional spacetime. The classical action of the lattice model in two-dimensional Minkowski spacetime is

$$S = \frac{1}{2} \int_{-\infty}^{\infty} dt \int_{0}^{L} dx \left[ \frac{\partial \phi^*}{\partial t} \frac{\partial \phi}{\partial t} - \frac{\partial \phi^*}{\partial x} \frac{\partial \phi}{\partial x} - m^2 |\phi|^2 \right]$$
$$- \frac{1}{4!} \int_{-\infty}^{\infty} dt \int_{0}^{L} dx dy |\phi(x, t)|^2 V(x - y) |\phi(y, t)|^2, \quad (4)$$

where the complex  $\phi(x,t)$  field operator describes a charged scalar particle of mass m, and it satisfies the periodic boundary condition

$$\phi(x+L,t) = \phi(x,t). \tag{5}$$

The short-range spatially symmetric instantaneous interaction potential is represented by V(x) = V(-x).

# A. Two-particle correlation function and its spectral representation

The two charged scalar particles interaction can be studied via evaluating the time dependence of the correlation function. The two-particle correlation function is defined by

$$C(rt; r'0) = \theta(t)\langle 0|\mathcal{O}(r, t)\mathcal{O}^{\dagger}(r', 0)|0\rangle + \theta(-t)\langle 0|\mathcal{O}^{\dagger}(r', 0)\mathcal{O}(r, t)|0\rangle,$$
(6)

where two identical charged particles creation operator after projecting out center of mass motion (CM) in the rest frame is given by

$$\mathcal{O}^{\dagger}(r,t) = \frac{1}{\sqrt{2}} \int_0^L \frac{dx_2}{\sqrt{L}} \phi(r+x_2,t) \phi(x_2,t).$$
 (7)

The factor  $1/\sqrt{2}$  takes into account the exchange symmetry of two distinguishable charged particles. Inserting the complete energy basis,  $\sum_n |E_n\rangle\langle E_n|=1$ , between interpolating operators, and defining the two-particle relative wave function by

$$\langle E_n | \mathcal{O}^{\dagger}(r', 0) | 0 \rangle = \frac{1}{\sqrt{L}} \frac{\psi_{E_n}^{(L)*}(r')}{E_n},$$
 (8)

similarly

$$\langle E_n | \mathcal{O}(r,t) | 0 \rangle = \frac{1}{\sqrt{L}} \frac{\psi_{E_n}^{(L)*}(r)}{E_n} e^{iE_n t} \tag{9}$$

defines the wave function of two-antiparticle states, where we have assumed that wave functions of two-particle and two-antiparticle are identical. The spectral representation of two-particle correlation function is thus given by

$$C(rt; r'0) = \frac{\theta(t)}{L} \sum_{n} \frac{\psi_{E_{n}}^{(L)}(r)}{E_{n}} \frac{\psi_{E_{n}}^{(L)*}(r')}{E_{n}} e^{-iE_{n}t} + \frac{\theta(-t)}{L} \sum_{n} \frac{\psi_{E_{n}}^{(L)}(r')}{E_{n}} \frac{\psi_{E_{n}}^{(L)*}(r')}{E_{n}} e^{iE_{n}t}.$$
(10)

The first and the second terms in Eq. (10) describe two-particle states propagating forward in time and two-anti-particle states propagating backward in time, respectively. In general, both parities contribute to energy states, for scalar particles considered in this work, only even parity energy states survived due to Bose symmetry,

$$\psi_{E_n}^{(L)}(-r) = \psi_{E_n}^{(L)}(r). \tag{11}$$

The noninteracting correlation function is given by

$$C_0(rt; r'0) = \frac{1}{L} \sum_{\substack{n = \frac{2\pi n}{n}, n \in \mathbb{Z}}} \frac{\cos(pr)}{E_p^{(0)}} \frac{\cos(pr')}{E_p^{(0)}} e^{-iE_p^{(0)}|t|}, \quad (12)$$

where free two-particle energies are  $E_p^{(0)} = 2\sqrt{p^2 + m^2}$  with  $p = \frac{2\pi n}{L}$ ,  $n \in \mathbb{Z}$ .

The two-particle relative wave function is required to satisfy the relativistic Lippmann-Schwinger (LS)-like equation; see, e.g., Appendixes A and B,

$$\psi_E^{(L)}(r) = \int_0^L dr' G_0^{(L)}(r - r'; E) V(r') \psi_E^{(L)}(r'). \tag{13}$$

The relativistic finite volume Green function is defined by (see, e.g., Refs. [17,39])

$$G_0^{(L)}(r;E) = \frac{1}{L} \sum_{q = \frac{2\pi n}{n}, n \in \mathbb{Z}} \frac{1}{\omega_q} \frac{e^{iqr}}{E^2 - (2\omega_q)^2}, \quad (14)$$

where  $\omega_q = \sqrt{q^2 + m^2}$  is the energy of a single particle with momentum q. The relativistic wave function is normalized in momentum space by

$$\frac{1}{L} \sum_{p=\frac{2\pi n}{n}} \frac{1}{n \in \mathbb{Z}} \frac{1}{2\omega_p} \tilde{\psi}_{E_n}^{(L)}(p) \tilde{\psi}_{E_{n'}}^{(L)*}(p) = E_n L \frac{\delta_{n,n'} + \delta_{n,-n'}}{2}, \quad (15)$$

where the Fourier transform of the wave function is defined by

$$\frac{\tilde{\psi}_{E_n}^{(L)}(p)}{2\omega_p} = \int_0^L dr \psi_{E_n}^{(L)}(r) e^{ipr}.$$
 (16)

Using the normalization relation of the wave function in Eq. (15), we find

$$\frac{1}{L} \sum_{\substack{p = \frac{2\pi n}{n}, n \in \mathbb{Z}}} 2\omega_p \tilde{C}(pt; p0) = \sum_{n=0}^{\infty} \frac{e^{-iE_n|t|}}{E_n}, \quad (17)$$

where the Fourier transform of the correlation function is defined by

$$\tilde{C}(pt; p'0) = \int_0^L dr dr' e^{ipr} C(rt; r'0) e^{-ip'r'}.$$
 (18)

Equation (17) may be considered as the integrated correlation function in momentum space. The difference of interacting and noninteracting integrated correlation functions is thus given by

$$\Delta C(t) = \frac{1}{L} \sum_{p = \frac{2\pi n}{L}, n \in \mathbb{Z}} 2\omega_p [\tilde{C}(pt; p0) - \tilde{C}_0(pt; p0)]$$

$$= \sum_{n=0}^{\infty} \left[ \frac{e^{-iE_n t}}{E_n} - \frac{e^{-iE_n^{(0)} t}}{E_n^{(0)}} \right]. \tag{19}$$

# B. Relating integrated correlation functions to the scattering phase shift

In momentum space, the two-particle correlation function along the diagonal direction is given by

 $\tilde{C}(pt; p0)$ 

$$= \frac{1}{L} \sum_{n} \frac{1}{E_{n}^{2}} \frac{\tilde{\psi}_{E_{n}}^{(L)}(p)}{E_{p}} \frac{\tilde{\psi}_{E_{n}}^{(L)*}(p)}{E_{p}} [\theta(t)e^{-iE_{n}t} + \theta(-t)e^{iE_{n}t}].$$
(20)

Using identity

$$i \int_{-\infty}^{\infty} \frac{d\lambda}{2\pi} \frac{e^{-i\lambda t}}{\lambda + i0} = \theta(t), \tag{21}$$

the particles time forward and antiparticles time backward propagations can be combined. The momentum space spectral representation of the two-particle correlation function along the diagonal direction is thus expressed in terms of the two-particle Green function by

$$\tilde{C}(pt; p0) = i \int_{-\infty}^{\infty} \frac{d\lambda}{2\pi} \tilde{G}^{(L)}(p, p; \lambda) e^{-i\lambda t}.$$
 (22)

The diagonal terms of the momentum space two-particle Green function is defined by

$$\tilde{G}^{(L)}(p,p;E) = \int_0^L dr dr' e^{ipr} G^{(L)}(r,r';E) e^{-ipr'}, \qquad (23)$$

where the two-particle Green function is given by

$$G^{(L)}(r,r';E) = \frac{1}{L} \sum_{q = \frac{2\pi\mu}{n}, n \in \mathbb{Z}} \frac{1}{\omega_q} \frac{\psi_{E_q}^{(L)}(r) \psi_{E_q}^{(L)*}(r')}{E^2 - E_q^2 + i0}, \quad (24)$$

and  $E_q=2\omega_q=2\sqrt{q^2+m^2}$ . Hence, the difference of integrated correlation functions is given in terms of Green's functions by

$$\Delta C(t) = i \int_{-\infty}^{\infty} \frac{d\lambda}{2\pi} e^{-i\lambda t} \times \frac{1}{L} \sum_{p = \frac{2\pi n}{L}, n \in \mathbb{Z}} 2\omega_p [\tilde{G}^{(L)}(p, p; \lambda) - \tilde{G}_0^{(L)}(p, p; \lambda)],$$
(25)

where the Fourier transform of Green's functions are defined in a similar way as in Eq. (18).

Next, using the relativistic Friedel formula relation in infinite volume (see Appendix A 3),

$$\int_{-\infty}^{\infty} \frac{dp}{2\pi} \omega_p \left[ \tilde{G}^{(\infty)}(p, p; E) - \tilde{G}_0^{(\infty)}(p, p; E) \right]$$

$$= -\frac{1}{\pi} \int_{4m^2}^{\infty} ds \frac{\delta(\sqrt{s})}{(s - E^2 - i0)^2}, \tag{26}$$

where  $\delta(E)$  is the scattering phase shift of two scalar particles, at a large volume limit, the difference of integrated correlation functions thus approaches

$$\Delta C(t) \stackrel{L \to \infty}{\to} -\frac{1}{\pi} \int_{4m^2}^{\infty} ds \delta(\sqrt{s}) \left[ i \int_{-\infty}^{\infty} \frac{d\lambda}{\pi} \frac{e^{-i\lambda t}}{(s - \lambda^2 - i0)^2} \right]. \tag{27}$$

Completing the integration in brackets, a compact form of the large volume limit of the difference of integrated correlation functions can be found,

$$\triangle C(t) \overset{L \to \infty}{\underset{t = -i\tau}{\longrightarrow}} -\frac{1}{\pi} \int_{2m}^{\infty} d\epsilon \delta(\epsilon) \frac{d}{d\epsilon} \left(\frac{e^{-\epsilon\tau}}{\epsilon}\right). \tag{28}$$

This relation that is also listed in Eq. (3) is our main result. Using an exactly solvable model and perturbation theory in Sec. II C and Sec. II D, respectively, we show that the difference of integrated correlation functions converges rapidly to its infinite volume limit.

## C. Exactly solvable model with a contact interaction

Considering a contact interaction,

$$V(r) = V_0 \delta(r), \tag{29}$$

the action in Eq. (4) is thus reduced to a complex scalar  $\phi^4$  theory action. The finite volume LS equation in Eq. (13) yields the quantization condition

$$\frac{1}{V_0} = G_0^{(L)}(0; E), \tag{30}$$

where finite volume free two-particle Green's function is defined in Eq. (14).

Using scattering solutions in infinite volume, Eqs. (A3) and (A8) in Appendix A, the potential strength  $V_0$  is related to infinite volume free particle Green's function by

$$\frac{1}{V_0} = \text{Re}[G_0^{(\infty)}(0; E)] - \rho(E)\cos \delta(E), \tag{31}$$

where the analytic expressions of  $G_0^{(\infty)}(0; E)$  and  $\rho(E)$  are given in Eqs. (A6) and (A7), respectively (see details in Appendix A). The quantization condition can be rewritten in a form that is known as the Lüscher formula,

$$\cos \delta(E) = \frac{\text{Re}[G_0^{(\infty)}(0; E)] - G_0^{(L)}(0; E)}{\rho(E)}.$$
 (32)

The right-hand side of Eq. (32) is typically referred to as a zeta function that is associated with the long-range geometry of a lattice (see, e.g., Ref. [4]). Let us rearrange the Lüscher formula to

$$\delta(E_n) + \phi(E_n) = n\pi, \tag{33}$$

where subscript-n in  $E_n$  is used to label the nth eigenenergy of the system, and

$$\phi(E) = -\cot^{-1} \left[ \frac{\text{Re}[G_0^{(\infty)}(0; E)] - G_0^{(L)}(0; E)}{\rho(E)} \right] + l\pi, \quad (34)$$

where  $l \in \mathbb{Z}$ . The  $l\pi$  is added to keep  $\phi(E)$  as a monotonic function and prevent jumping at branch points when  $E = 2\sqrt{(\frac{2\pi n}{L})^2 + m^2}$  where  $n \in \mathbb{Z}$  [see, e.g., Fig. 1(a)]. The fast convergence of relation

$$\sum_{n=0}^{\infty} \left[ \frac{e^{-E_n \tau}}{E_n} - \frac{e^{-E_n^{(0)} \tau}}{E_n^{(0)}} \right] \stackrel{L \to \infty}{\to} -\frac{1}{\pi} \int_{2m}^{\infty} d\epsilon \delta(\epsilon) \frac{d}{d\epsilon} \left( \frac{e^{-\epsilon \tau}}{\epsilon} \right)$$
(35)

can be verified numerically, where interacting energy levels are determined by the quantization condition in Eq. (33). The free particles energy levels are given by  $E_n^{(0)} = 2\sqrt{(\frac{2\pi n}{L})^2 + m^2}$ . The phase shift is computed by

using Eq. (31). The difference of the finite volume integrated correlation functions approaches its infinite volume limit rapidly [see, e.g., Fig. 1(b)].

# D. Leading order result of the perturbation calculation

The fast convergence of the difference of integrated correlation functions to its infinite volume limit can also be checked straightforwardly by perturbation theory. The perturbation calculation can be carried out in a similar way as demonstrated in Ref. [58], and the leading order contribution is given by

$$C(r,t;r',0) - C_0(r,t;r',0)$$

$$= -\frac{iV_0}{L} \int_0^L dx_2 \int_0^L dx_2' \int_{-\infty}^\infty dt' \int_0^L dx''$$

$$\times D_0^{-1}(r + x_2 - x'', t - t'') D_0^{-1}(x_2 - x'', t - t'')$$

$$\times D_0^{-1}(x'' - r' - x_2', t'') D_0^{-1}(x'' - x_2', t'') + \mathcal{O}(V_0^2), \quad (36)$$

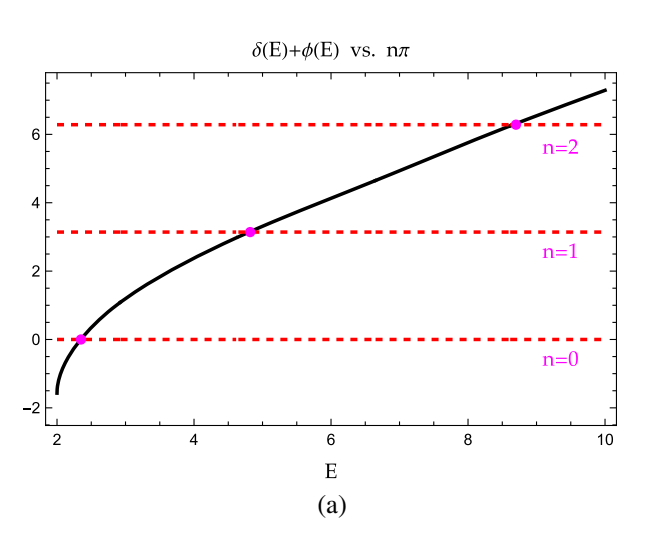
where the free two-particle propagator is defined by

$$D_0^{-1}(x,t) = i \int_{-\infty}^{\infty} \frac{d\epsilon}{2\pi} \frac{1}{L} \sum_{k=\frac{2\pi n}{L}, n \in \mathbb{Z}} \frac{e^{ikx} e^{i\epsilon t}}{\epsilon^2 - (k^2 + m^2)}.$$
 (37)

Carrying out space and time integration, we find

$$C(r, t; r', 0) - C_0(r, t; r', 0)$$

$$= -iV_0 \int_{-\infty}^{\infty} \frac{d\epsilon}{2\pi} e^{i\epsilon t} G_0^{(L)}(r; \epsilon) G_0^{(L)}(r'; \epsilon) + \mathcal{O}(V_0^2), \quad (38)$$



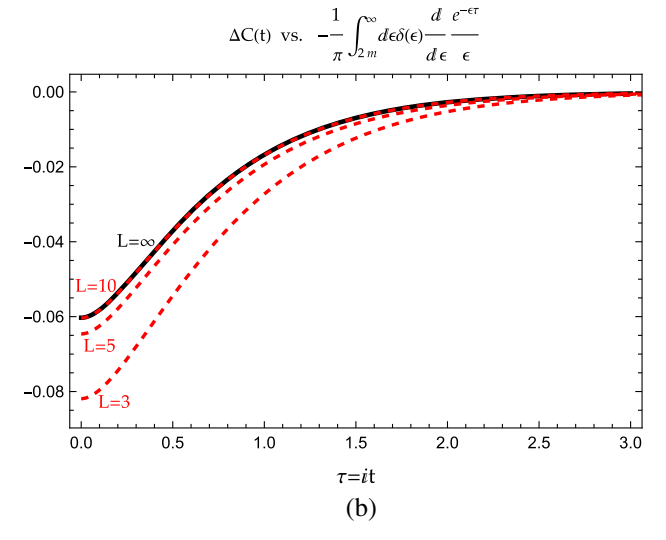


FIG. 1. The energy spectra and difference of integrated correlation function plots: (a)  $\delta(\epsilon_n) + \phi(\epsilon_n)$  (solid black curves vs  $n\pi$  (dashed red lines) with L=3, and energy spectra are located at intersection points of black and red curves; (b)  $-\frac{1}{\pi}\int_{2m}^{\infty}d\epsilon\delta(\epsilon)\frac{d}{d\epsilon}(\frac{e^{-\epsilon\tau}}{\epsilon})$  (solid black curve) vs  $\Delta C(t) = \sum_{n=0}^{\infty} \left[\frac{e^{-E_n\tau}}{E_n} - \frac{e^{-E_n^{(0)}\tau}}{E_n^{(0)}}\right]$  (dashed red curves) with L=3, 5, 10. The rest of the parameters are taken as m=1 and  $V_0=5$ .

where the finite volume free particles Green function,  $G_0^{(L)}(r;\epsilon)$ , is defined in Eq. (14). Using the definition of the difference of integrated correlation functions in Eq. (19) and further carrying out the integration of  $\epsilon$ , the leading order result of the perturbation calculation is given by

$$\Delta C(t)^{t=-i\tau} - \frac{V_0}{L} \sum_{k=\frac{2\pi n}{2}, n \in \mathbb{Z}} \frac{\tau + \frac{1}{E_k}}{E_k^3} e^{-E_k \tau} + \mathcal{O}(V_0^2), \quad (39)$$

where again  $E_k = 2\sqrt{k^2 + m^2}$  is the total energy of two particles. At the large volume limit, it thus approaches

$$\Delta C(t) \xrightarrow[t=-i\tau]{L\to\infty} -V_0 \int_{-\infty}^{\infty} \frac{dk}{2\pi} \frac{\tau + \frac{1}{E_k}}{E_k^3} e^{-E_k \tau} + \mathcal{O}(V_0^2). \tag{40}$$

On the other hand, using the Taylor expansion of scattering phase shift,

$$\delta(E_k) = -\frac{V_0}{4kE_k} + \mathcal{O}(V_0^2), \tag{41}$$

we thus find

$$-\frac{1}{\pi} \int_{2m}^{\infty} d\epsilon \delta(\epsilon) \frac{d}{d\epsilon} \left( \frac{e^{-\epsilon \tau}}{\epsilon} \right)$$

$$= -V_0 \int_{-\infty}^{\infty} \frac{dk}{2\pi} \left( \tau + \frac{1}{\epsilon_k} \right) \frac{e^{-\epsilon_k \tau}}{\epsilon_k^3} + \mathcal{O}(V_0^2), \quad (42)$$

where  $\epsilon_k = 2\sqrt{k^2 + m^2}$ . This is indeed consistent with perturbation calculation.

# III. MONTE CARLO SIMULATION OF THE COMPLEX $\phi^4$ LATTICE MODEL

In this section, the formalism is tested by carrying out the Monte Carlos simulation of the complex  $\phi^4$  lattice model, which describes charged scalar particles interacting with a contact potential. The results are compared with the result by using the Lüscher formula. The Euclidean spacetime lattice  $\phi^4$  action is given by (see, e.g., Ref. [35])

$$S_{E} = -\kappa \sum_{x,\tau,\hat{n}_{x},\hat{n}_{\tau}} \hat{\phi}^{*}(x,\tau) \hat{\phi}(x+\hat{n}_{x},\tau+\hat{n}_{\tau}) + \text{c.c.}$$

$$+ (1-2\lambda) \sum_{x,\tau} |\hat{\phi}(x,\tau)|^{2} + \lambda \sum_{x,\tau} |\hat{\phi}(x,\tau)|^{4}, \qquad (43)$$

where  $(x,\tau)$  refer to discrete coordinates of the Euclidean  $L\times T$  lattice site:  $x\in [0,L-1]$  and  $\tau\in [0,T-1]$ . The lattice spacing, a, is set to unity. The  $(\hat{n}_x,\hat{n}_\tau)$  denotes the unit vector in direction  $(x,\tau)$  on a periodic square lattice. The parameters  $(\kappa,\lambda)$  are related to bare mass  $m_0$  and bare coupling constant  $g_0$  of interacting term  $\frac{g_0}{4!}|\phi|^4$  by  $m_0^2=\frac{1-2\lambda}{\kappa}-8$  and  $g_0=\frac{6\lambda}{\kappa^2}$  (see Ref. [35]). The  $\phi$  field in the

 $\phi^4$  lattice model has been rescaled:

$$\phi(x,\tau) = \sqrt{2\kappa}\hat{\phi}(x,\tau).$$

The numerical simulation is carried out by the hybrid Monte Carlo (HMC) algorithm, and the details of the HMC algorithm are described in Ref. [35].

The single-particle and two-particle correlation functions are defined, respectively, by

$$C^{(\phi)}(x\tau, x'0) = \frac{\int \mathcal{D}\phi \mathcal{D}\phi^{\dagger}\phi(x, \tau)\phi^{\dagger}(x', 0)e^{-S_E}}{\int \mathcal{D}\phi \mathcal{D}\phi^{\dagger}e^{-S_E}}$$
(44)

and

$$C^{(2\phi)}(r\tau, r'0) = \frac{\int \mathcal{D}\phi \mathcal{D}\phi^{\dagger} \mathcal{O}(r, \tau) \mathcal{O}^{\dagger}(r', 0) e^{-S_E}}{\int \mathcal{D}\phi \mathcal{D}\phi^{\dagger} e^{-S_E}}, \quad (45)$$

where the relative motion of the two-particle interpolating operator is defined in Eq. (7).

The individual energy levels can be projected out by

$$\tilde{C}^{(\phi,2\phi)}(p,\tau) = \sum_{x,x' \in [0,L-1]} e^{ipx} C^{(\phi,2\phi)}(x\tau,x'0) e^{-ipx'}, \quad (46)$$

where 
$$p = \frac{2\pi n}{L}, n \in [-\frac{L}{2} + 1, \frac{L}{2}].$$

## A. Simulation test for the noninteracting case: $\lambda = 0$

For noninteracting particles by setting  $\lambda = 0$  in the Euclidean action in Eq. (43), the analytic expression of the correlation functions can be found. The single-particle correlation is given by

$$C_0^{(\phi)}(x\tau, x'0) = \frac{1}{L} \sum_{k=\frac{2\pi n}{2}}^{n \in \left[\frac{-L}{2} + 1, \frac{L}{2}\right]} e^{ik(x-x')} G_{\phi}(k, \tau), \quad (47)$$

and the two-particle correlation function is given by

$$C_0^{(2\phi)}(r\tau, r'0) = \frac{1}{L} \sum_{k=\frac{2\pi n}{L}}^{n \in \left[-\frac{L}{2} + 1, \frac{L}{2}\right]} \cos(kr) \cos(kr') [G_{\phi}(k, \tau)]^2,$$
(48)

where

$$G_{\phi}(k,\tau) = \frac{1}{T} \sum_{\omega = \frac{2\pi n}{T}}^{n \in [0,T-1]} \frac{e^{i\omega\tau}}{2 - 2\cos\omega - 2\cos k + 2\cosh m}.$$
(49)

In the above expressions, the lattice spacing a has been set to unity, and the lattice spacing can be installed easily, such as by replacing  $\omega$  by the dimensionless argument in

 $\cos(a\omega)$ . At the limit of  $T \to \infty$  and also taking lattice spacing to zero  $(a \to 0)$ , we find

$$G_{\phi}(k,\tau) \stackrel{T \to \infty}{\underset{a \to 0}{\to}} \frac{e^{-\omega_k \tau}}{2\omega_k},$$
 (50)

and single and two-particle correlation functions approach

$$C_0^{(\phi)}(x\tau, x'0) \stackrel{T \to \infty}{\underset{a \to 0}{\to}} \frac{1}{L} \sum_{k = \frac{2\pi n}{2}}^{n \in \mathbb{Z}} e^{ik(x - x')} \frac{e^{-\omega_k \tau}}{2\omega_k}$$
 (51)

and

$$C_0^{(2\phi)}(x\tau, x'0) \overset{T \to \infty}{\underset{a \to 0}{\to}} \frac{1}{L} \sum_{k=\frac{2\pi n}{2}}^{n \in \mathbb{Z}} \cos(kr) \cos(kr') \frac{e^{-2\omega_k \tau}}{(2\omega_k)^2}, \quad (52)$$

where 
$$\omega_k = \sqrt{k^2 + m^2}$$
.

The individual energy level can be extracted by projecting the correlation functions into momentum space along the diagonal direction,

$$\tilde{C}_0^{(\phi,2\phi)}(p,\tau) = \sum_{x,x' \in [0,L-1]} e^{ipx} C_0^{(\phi,2\phi)}(x\tau,x'0) e^{-ipx'}, \quad (53)$$

and, thus, we find

$$\frac{1}{L}\tilde{C}_{0}^{(\phi)}(p,\tau) = G_{\phi}(p,\tau) \stackrel{T \to \infty}{\underset{a \to 0}{\to}} \frac{e^{-\omega_{p}\tau}}{2\omega_{p}}, \tag{54}$$

where  $p = \frac{2\pi n}{L}$ ,  $n \in \left[-\frac{L}{2} + 1, \frac{L}{2}\right]$ , and

$$\frac{1}{L}\tilde{C}_0^{(2\phi)}(p,\tau) = \frac{\sigma_p}{2} \left[ G_\phi(p,\tau) \right]^2 \stackrel{T \to \infty}{\underset{a \to 0}{\to}} \frac{\sigma_p}{2} \frac{e^{-2\omega_p \tau}}{(2\omega_p)^2}, \quad (55)$$

where the symmetry factor  $\sigma_p$  is defined by

$$\sigma_p = \begin{cases} 2, & \text{if } p = 0, \\ \frac{1}{2}, & \text{if } p = \pi, \\ 1, & \text{otherwise.} \end{cases}$$
 (56)

At the limit of  $a \to 0$  and  $T \to \infty$ , the integrated correlation functions of free particles approach

$$C_0^{(\phi)}(\tau) = \frac{1}{L} \sum_{p = \frac{2\pi n}{L}}^{n \in \left[-\frac{L}{2} + 1, \frac{L}{2}\right]} \tilde{C}_0^{(\phi)}(p, \tau) \xrightarrow[a \to 0]{T \to \infty} \sum_{p = \frac{2\pi n}{L}}^{n \in \mathbb{Z}} \frac{e^{-\omega_p \tau}}{2\omega_p}$$
(57)

and

$$C_0^{(2\phi)}(\tau) = \frac{1}{L} \sum_{p=\frac{2\pi n}{L}}^{n \in [-\frac{L}{2}+1,\frac{L}{2}]} 2\omega_p^{(a,L)} \tilde{C}_0^{(2\phi)}(p,\tau)$$

$$\xrightarrow{T \to \infty} \sum_{a\to 0}^{n \in [0,\infty]} \frac{e^{-2\omega_p \tau}}{2\omega_p}, \tag{58}$$

where

$$\omega_p^{(a,L)} = \cosh^{-1}[1 + \cosh m - \cos p] \stackrel{a \to 0}{\to} \sqrt{p^2 + m^2}.$$
 (59)

The simulations for noninteracting charged scalar particles are performed with the choice of the parameters:  $\kappa=0.1213$ , and  $\lambda=0$ . The temporal extent of the lattice and the spatial extent of the lattice are fixed at T=100 and L=80, respectively. For each set of lattice, one million measurements are generated.

The mass of a single particle is measured by fitting projected single-particle correlation function  $\tilde{C}_0^{(\phi)}(p,\tau)$  with p=0, and we find  $m=0.3502\pm0.0032$ . Using the single particle's mass as input, the comparison of the analytic expression of effective mass, where

$$m_{\text{eff}}^{(\phi,2\phi)}(p,\tau) = \ln \frac{\tilde{C}_0^{(\phi,2\phi)}(p,\tau)}{\tilde{C}_0^{(\phi,2\phi)}(p,\tau+1)},$$
 (60)

vs lattice data are plotted in Figs. 2(a) and 2(c). The plots of projected single-particle and two-particle correlation functions  $\tilde{C}_0^{(\phi,2\phi)}(p,\tau)$  that are defined in Eqs. (54) and (55) vs lattice data are shown in Figs. 2(b) and 2(d). The plots of integrated correlation functions,  $C_0^{(\phi,2\phi)}(\tau)/L$ , that are defined in Eqs. (57) and (58), vs lattice data are shown in Figs. 3(a) and 3(c). We also plot  $1-C_0^{(\phi,2\phi)}(\tau)/C_{\rm lat}^{(\phi,2\phi)}(\tau)$  in Figs. 3(b) and 3(d) to illustrate good agreement between lattice data and analytic expression of free single-particle and two-particle correlation functions.

#### B. Contact interacting cases: $\lambda \neq 0$

# 1. Extracting phase shift from integrated correlation function

The simulations for interacting charged scalar particles are performed with the choice of the parameters:  $\kappa = 0.1286$ , and  $\lambda = 0.01$ . The temporal extent of the lattice is fixed at T = 120, and various spatial extents of lattice L's are computed.

The mass of a single particle is measured by fitting projected single-particle correlation function  $\tilde{C}_0^{(\phi)}(p,\tau)$  with p=0, where we find  $m \approx 0.2720 \pm 0.0015$ . The examples of the single-particle effective mass of lattice data are plotted in Fig. 4(a), and the single-particle mass as a function of lattice size L is

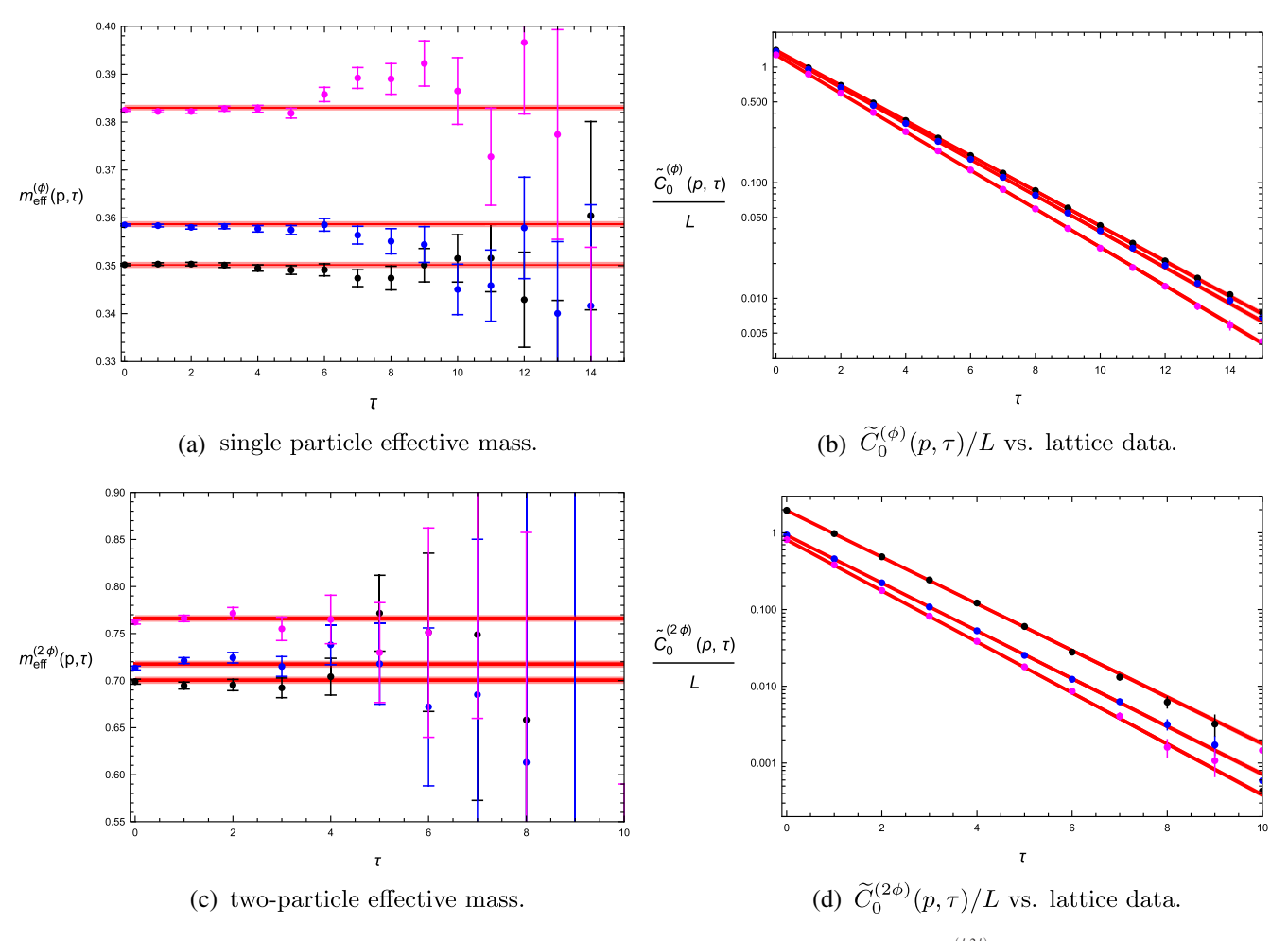


FIG. 2. Comparison of (a),(c) single-particle and two-particle effective mass  $m_{\text{eff}}^{(\phi,2\phi)}(p,\tau) = \ln \frac{\bar{C}_0^{(\phi,2\phi)}(p,\tau)}{\bar{C}_0^{(\phi,2\phi)}(p,\tau+1)}$  (red band) vs lattice data, where  $p = \frac{2\pi n}{L}$ , n = 0 (black error bars), 1 (blue error bars), and 2 (purple error bars); (b),(d)  $\frac{\bar{C}_0^{(\phi,2\phi)}(p,\tau)}{L}$  (red band) vs lattice data, where  $p = \frac{2\pi n}{L}$ , n = 0 (black error bars), 1 (blue error bars), and 2 (purple error bars). The model parameters are taken as  $\kappa = 0.1213$ ,  $\lambda = 0$ , T = 100, and L = 80.

$$m(L) = m + \frac{c}{\sqrt{L}}e^{-mL},\tag{61}$$

where  $m=0.272\pm0.0015$  and  $c=0.31\pm0.05$ , in Fig. 4(c). The plot of the integrated single-particle correlation function vs data,  $1-C_0^{(\phi)}(\tau)/C_{\rm lat}^{(\phi)}(\tau)$ , is shown in Fig. 4(b). The difference of integrated two-particle correlation functions between lattice data and the noninteracting analytic expression,  $\Delta C^{(2\phi)}(\tau)$ , is plotted in Fig. 4(d), where  $\Delta C^{(2\phi)}(\tau)$  is defined by

$$\Delta C^{(2\phi)}(\tau) = C_{\text{lat}}^{(2\phi)}(\tau) - C_0^{(2\phi)}(\tau)$$
 (62)

and

$$C_{\text{lat}}^{(2\phi)}(\tau) = \frac{1}{L} \sum_{p=\frac{2\pi n}{2}}^{n \in [-\frac{L}{2}+1,\frac{L}{2}]} 2\omega_p^{(a,L)} \tilde{C}_{\text{lat}}^{(2\phi)}(p,\tau).$$
 (63)

The analytical expression of noninteracting particles correlation function  $C_0^{(2\phi)}(\tau)$  is defined in Eq. (58), and  $\omega_p^{(a,L)}$  is defined in Eq. (59). The contact interaction coupling strength can be extracted from  $\Delta C^{(2\phi)}(\tau)$  [see Fig. 4(d)], and we find

$$V_0 = 0.196 \pm 0.030. \tag{64}$$

Similar to the nonrelativistic case [58], both interacting and noninteracting particles correlation functions are divergent as  $L \to \infty$  and  $\tau \sim 0$ , where the divergent part behaves as  $C_{\rm lat}^{(2\phi)}(\tau \sim 0) \propto L$  ln L. The divergent parts are canceled out so that  $\Delta C^{(2\phi)}(\tau)$  remains well behaved as  $L \to \infty$ . The cancellation of divergence is crucial; hence, the accurate representation of  $C_0^{(2\phi)}(\tau)$  is important. The consequence is that  $\Delta C^{(2\phi)}(\tau)$  is sensitive to the mass of the  $\phi$  field near small Euclidean time that ultimately generates large uncertainties near  $\tau \sim 0$ .

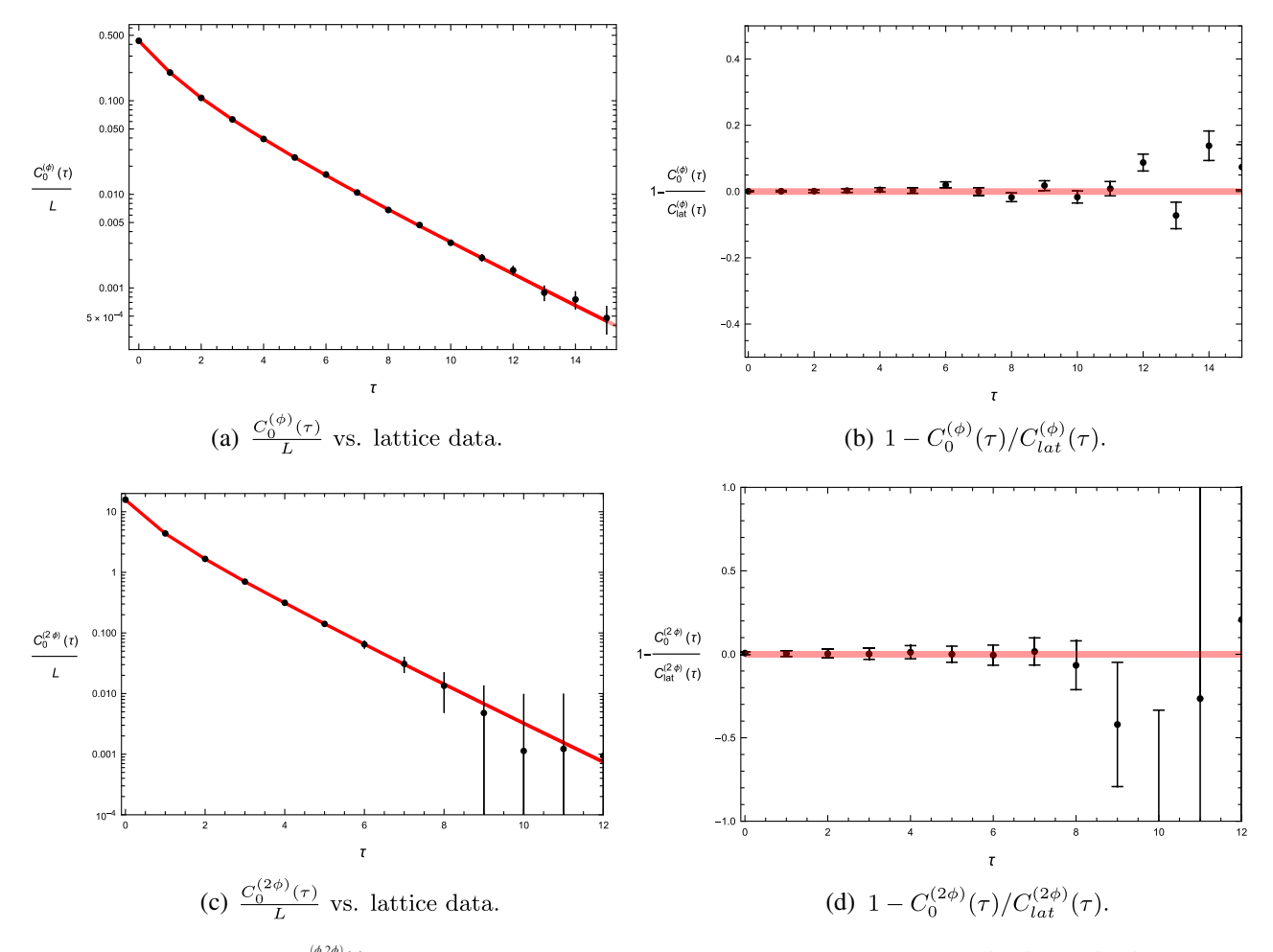


FIG. 3. (a),(c) Comparison of  $\frac{C_0^{(\phi,2\phi)}(\tau)}{L}$  (red band) vs lattice data (black error bars); (b),(d) plot of  $1-C_0^{(\phi,2\phi)}(\tau)/C_{\text{lat}}^{(\phi,2\phi)}(\tau)$  (black error bars); the red error band is also plotted. The model parameters are taken as  $\kappa=0.1213$ ,  $\lambda=0$ , T=100, and L=80.

## 2. Comparison with the Lüscher formula result

The individual two-particle energy levels can be extracted by applying the generalized eigenvalue method [59]

$$\tilde{C}^{(2\phi)}(\tau)\xi_n = \lambda_n(\tau,\tau_0)\tilde{C}^{(2\phi)}(\tau_0)\xi_n, \tag{65}$$

where  $\tau_0$  is a small reference time and is set to zero in this work. The two-particle correlation function matrices is defined by

$$[\tilde{C}^{(2\phi)}(\tau)]_{p,p'} = \sum_{x,x' \in [0,L-1]} e^{ipx} C^{(2\phi)}(x\tau,x'0) e^{-ip'x'}.$$
 (66)

A simple form of  $\lambda_n(\tau,0)=e^{-E_n\tau}$  is used in the data fitting for  $\tau\in[0,8]$ ; see the example of the effective mass of two-particle data in Fig. 5(a). To extract the scattering phase shift or coupling strength for the contact interaction, the two-particle lattice energy spectra are fitted by using the Lüscher formula.

Two different versions of quantization conditions are used in this work: first of all, the zero lattice spacing limit version of the quantization condition in Eq. (33) that is nothing but the Lüscher formula. Second, we also use the finite lattice spacing version of the quantization condition by taking into consideration the finite lattice spacing effect (a = 1)

$$\frac{1}{V_0} = G_0^{(a,L)}(0,E),\tag{67}$$

where

$$G_0^{(a,L)}(0,E) = \frac{1}{L} \sum_{p=\frac{2\pi n}{L}}^{n \in [-\frac{L}{2}+1,\frac{L}{2}]} \frac{1}{\omega_p^{(a,L)}} \frac{1}{E^2 - (2\omega_p^{(a,L)})^2}.$$
 (68)

As described in Sec. II C, Eq. (67) can be rewritten to the familiar Lüscher formula form. Two versions of quantization conditions make a negligible difference at low-lying energy spectra [see, e.g., Fig. 5(b)]. The value of the coupling strength extracted from lattice data is

$$V_0 = 0.165 \pm 0.040,$$

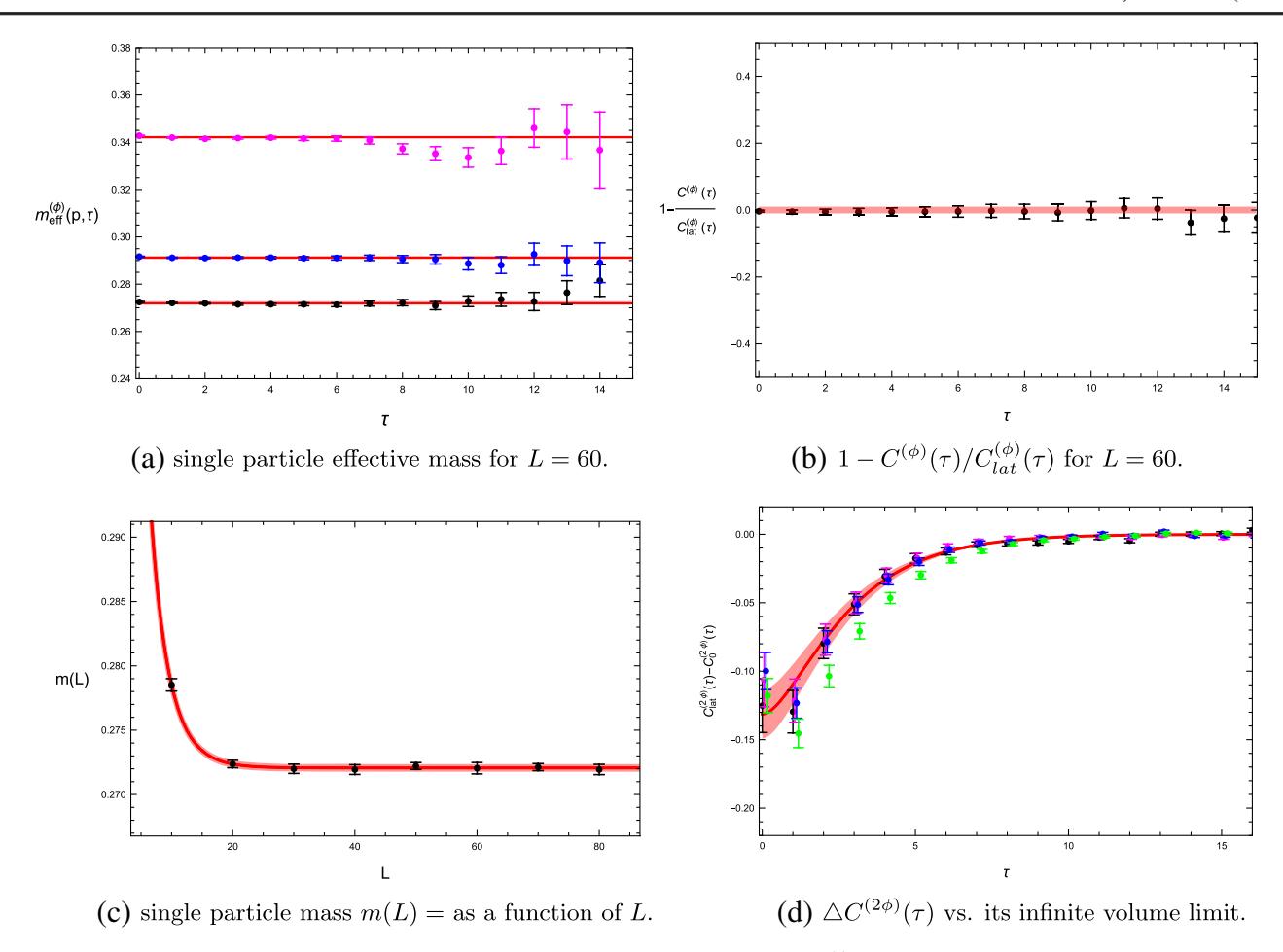


FIG. 4. (a) Plot of single-particle and two-particle effective mass  $m_{\text{eff}}^{(\phi)}(p,\tau) = \ln \frac{\tilde{C}_{\text{in}}^{(\phi)}(p,\tau)}{\tilde{C}_{\text{in}}^{(\phi)}(p,\tau+1)}$ , where  $p = \frac{2\pi n}{L}$ , n = 0 (black error bars), 1 (blue error bars), and 2 (purple error bars). The red dashed lines represent the free particles energy level, and the solid red lines and red bands are the center value and its error band of interacting energy levels. (b) Plot of  $1 - C_0^{(\phi)}(\tau)/C_{\text{lat}}^{(\phi)}(\tau)$  (black error bars), and the red error band is also plotted. (c) Single-particle mass as a function of lattice size L,  $m(L) = m + \frac{c}{\sqrt{L}}e^{-mL}$ , where  $m = 0.272 \pm 0.0015$  and  $c = 0.31 \pm 0.05$ . (d) Plot of  $\Delta C^{(2\phi)}(\tau)$  for lattice data with various L's ranging from L = 10 (green error bars), 20 (blue error bars), 30 (magenta error bars), and 40 (black error bars) vs its infinite volume limit (solid red curve and red band). The lattice data are plotted off-site horizontally for better visualization. The model parameters are taken as  $\kappa = 0.1286$ ,  $\lambda = 0.01$ , and T = 120.

which is slightly lower than the value by fitting the difference of integrated correlation functions.

## 3. Spectral representation check

As a consistent check, we also compute the difference of integrated two-particle correlation functions by its spectral representation

$$\Delta C^{(2\phi)}(\tau) \simeq \sum_{p=\frac{2\pi n}{L}}^{n \in \left[-\frac{L}{2} + 1, \frac{L}{2}\right]} \frac{\sigma_{p}}{2} \left[ \frac{e^{-E_{p}^{(a,L)}\tau}}{E_{p}^{(a,L)}} - \frac{e^{-2\omega_{p}^{(a,L)}\tau}}{2\omega_{p}^{(a,L)}} \right]$$

$$\stackrel{T \to \infty}{\underset{a \to 0}{\longrightarrow}} \sum_{p=\frac{2\pi n}{L}}^{n \in [0,\infty]} \left[ \frac{e^{-E_{p}\tau}}{E_{p}} - \frac{e^{-E_{p}^{(0)}\tau}}{E_{p}^{(0)}} \right], \tag{69}$$

where the finite volume energy levels are determined by the quantization condition in Eq. (67) or the Lüscher formula at the zero lattice spacing limit in Eq. (33). In terms of spectral representation results, we observe that the lattice data seem to prefer the value of the coupling strength,  $V_0 = 0.196 \pm 0.030$ , which is extracted from the integrated correlation function in Sec. III B 1. The spectral representation of  $\triangle C^{(2\phi)}(\tau)$  with  $V_0 \sim 0.196$  agrees well with lattice data. The example of the comparison of  $\triangle C^{(2\phi)}(\tau)$  by spectral representation vs the lattice data result is shown in Figs. 6(a) and 6(b), where the result of using the zero lattice spacing limit version of the Lüscher formula in Eq. (33) is also plotted in Fig. 6(a). Again, the finite lattice spacing quantization condition in Eq. (67) and the zero lattice spacing limit version of the quantization condition in Eq. (33) make negligible

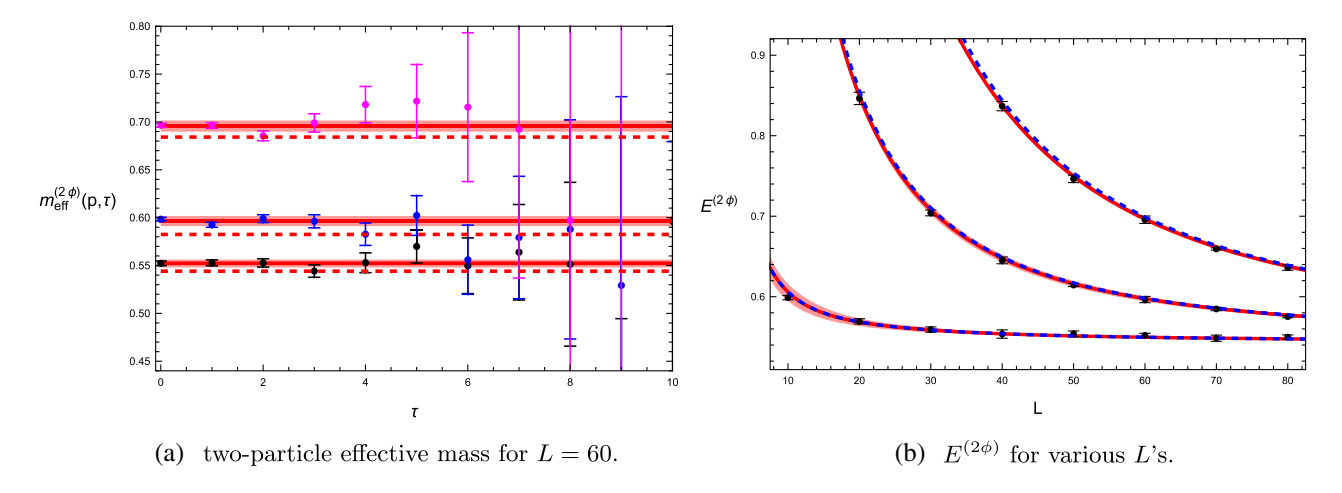


FIG. 5. (a) Plot of two-particle effective mass  $m_{\text{eff}}^{(2\phi)}(p,\tau) = \ln \frac{\tilde{C}_{\text{lat}}^{(2\phi)}(p,\tau)}{\tilde{C}_{\text{lat}}^{(2\phi)}(p,\tau+1)}$ , where  $p = \frac{2\pi n}{L}$ , n = 0 (black error bars), 1 (blue error bars), and 2 (purple error bars). The red dashed lines represent free particles energy level; solid red lines and red bands are the center value and its error band of interacting energy levels. (b) Comparison of two-particle energy spectra lattice data vs the Lüscher formula by using  $G_0^{(a,L)}(0,E)$  (red dashed curve), and vs the Lüscher formula result by using the zero lattice spacing version of  $G_0^{(L)}(0,E)$  (blue dashed curve). The model parameters are taken as  $\kappa = 0.1286$ ,  $\lambda = 0.01$ , T = 120, m = 0.272, and  $V_0 = 0.165 \pm 0.04$ .

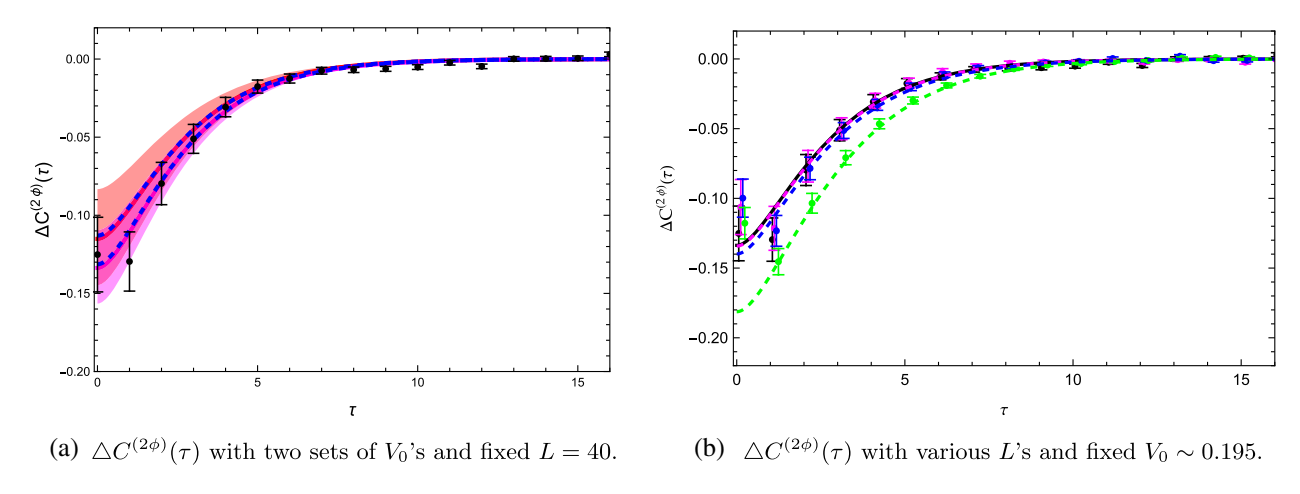


FIG. 6. (a) Comparison of  $\triangle C^{(2\phi)}(\tau)$  by using spectral representation in Eq. (69) vs the lattice result (black error bars) for two sets of  $V_0$ 's:  $V_0=0.196\pm0.030$  (purple) and  $V_0=0.165\pm0.040$  (red). The blue dashed curve is produced by using the zero finite spacing limit version of the Lüscher formula in Eq. (33). (b) Comparison of spectral representation of  $\triangle C^{(2\phi)}(\tau)$  with various L's for fixed  $V_0=0.196\pm0.030$ : L=10 (green error bars), 20 (blue error bars), 30 (purple error bars), and 40 (black error bars) vs lattice data. Only the center value curves are plotted. The model parameters are taken as T=120 and m=0.272.

difference in spectral representation results. The patten of convergence of both lattice data and spectral representation of  $\Delta C^{(2\phi)}(\tau)$  as increasing L is displayed in Fig. 6(b).

#### 4. A short summary

With the set of lattice model parameters  $\kappa = 0.1286$  and  $\lambda = 0.01$ , the difference of integrated correlation functions,  $\Delta C_{\rm lat}^{(2\phi)}(\tau)$ , for various *L*'s and a fixed T=120 are computed. The mass of the  $\phi$  field is  $m \sim 0.272$ . The

convergence of  $\triangle C_{\text{lat}}^{(2\phi)}(\tau)$  is observed and displayed in Figs. 4(d) and 6(b).

The coupling strength of the contact interaction potential is extracted by two different approaches:

- (1) Fitting lattice data of  $\Delta C_{\rm lat}^{(2\phi)}(\tau)$  with its infinite volume limit form in the right-hand side of Eq. (3), we find the value of coupling strength:  $V_0 = 0.196 \pm 0.030$  [see Fig. 4(d)].
- (2) The low-lying two-particle energy levels with various L's ranging from L = 10 up to 80 are extracted from projected two-particle correlation functions,

and then fitting lattice data of low-lying energy levels by using the quantization condition in Eq. (67), the coupling strength is thus extracted:  $V_0 = 0.165 \pm 0.040$  [see Fig. 5(b)].

(3) The spectral representation of  $\triangle C^{(2\phi)}(\tau)$  in Eq. (69) is also computed with  $V_0=0.196$  and plotted in Fig. 6(b).

Overall, the result by using the Lüscher formula to fit low-lying energy spectra and the result by fitting  $\triangle C^{(2\phi)}(\tau)$  agree with each other within errors. The possible cause on the difference of  $V_0$ 's from two approaches may be that the Lüscher formula fits only low-lying energy spectra; however, the integrated correlation function is the result of summing all energy levels. Fitting the difference of integrated correlation functions is more like a "global fit." In principle, the lattice data in the integrated correlation function contain inelastic contributions as well; however, the main result in Eq. (3) is only formulated based on the assumption of the existence of the elastic channel. The inelastic contributions are suppressed by exponentially decaying factor  $\frac{e^{-E_n t}}{E_n}$  for large  $\tau$ . However, since the mass of the single  $\phi$  field is only  $m \sim 0.272$ , the four-particle threshold starts at  $4m \sim 1.1$ , which is not too heavy; they may still have some residual effects near  $\tau \sim 0$ . The data in Figs. 4(d) and 6(b) near  $\tau \sim 0$  start going wild, which may be the indication of an inelastic contribution.

We remark that for the simple (1+1)-dimensional lattice model with a contact or short-range interaction potential, the scattering phase shift can be parametrized by a single parameter,  $V_0$ , which represents the strength of the short-range potential:

$$\delta(E) = \cot^{-1} \left[ \frac{\text{Re}[G_0^{(\infty)}(0; E)] - \frac{1}{V_0}}{\rho(E)} \right], \tag{70}$$

where the analytic expression of  $G_0^{(\infty)}(0;E)$  is given in Eq. (A6). In 1+1 dimensions, the contact interaction potential strength,  $V_0$ , is free of ultraviolet divergence, so it is convenient to use it as a free parameter for the scattering phase shift directly at the scope of current discussion. In general, the scattering phase shift is usually parametrized in terms of a few free parameters and kinematic factors based on either chiral perturbation theory or K-matrix formalism (see, e.g., [24,25]). The free parameters of the analytic form of the scattering phase shift can be associated with the renormalized coupling strength, mass of resonance, etc. For instance, the coupling strength of the contact interaction potential in 3 + 1 dimensions suffers ultraviolet divergence and must be renormalized, and the parametrization of the scattering phase shift is hence given in terms of the renormalized coupling strength [see, e.g., Eq. (75) in [17]].

#### C. Sanity check on inelastic contribution

As another sanity check about consistency between the Lüscher formula and the fitting  $\triangle C^{(2\phi)}(\tau)$  approach, two possible ways of suppressing inelastic channel contribution may be the following: (1) reducing coupling strength, since a four-particle contribution may start at the order of  $V_0^2$ ; and (2) increasing the mass of the  $\phi$  field; hence, the threshold of the four-particle contribution is lifted and the inelastic contribution is suppressed by  $\frac{e^{-E_n\tau}}{E_n}$  factors.

## 1. Perturbation calculation check

First of all, we reduce the coupling strength and compare results from the lowest order perturbation calculation, spectral representation of  $\Delta C^{(2\phi)}(\tau)$  in Eq. (69), and also the low-lying two-particle spectra. The lattice model parameters are reset to  $\kappa=0.1235$  and  $\lambda=0.001.$  The single-particle mass and coupling strength now are around  $m=0.267\pm0.002$  and  $V_0=0.025\pm0.008,$  respectively.

The perturbation calculation in Euclidean spacetime can be carried out as described in Sec. II D, also taking into consideration the finite lattice spacing, and we find

$$\Delta C_{\text{pert}}^{(2\phi)}(\tau) = \frac{1}{L} \sum_{p=\frac{2\pi n}{L}}^{n \in \left[\frac{L}{2}+1,\frac{L}{2}\right]} 2\omega_p^{(a,L)} \Delta \tilde{C}_{\text{pert}}^{(2\phi)}(p,\tau), \qquad (71)$$

where

$$\Delta \tilde{C}_{\text{pert}}^{(2\phi)}(p,\tau) = -\frac{V_0}{T} \sum_{\omega = \frac{2\pi n}{L}}^{n \in [0,T-1]} e^{i\omega\tau} [G_{2\phi}(p,\omega)]^2, \quad (72)$$

and the finite volume two-particle Green function is defined by

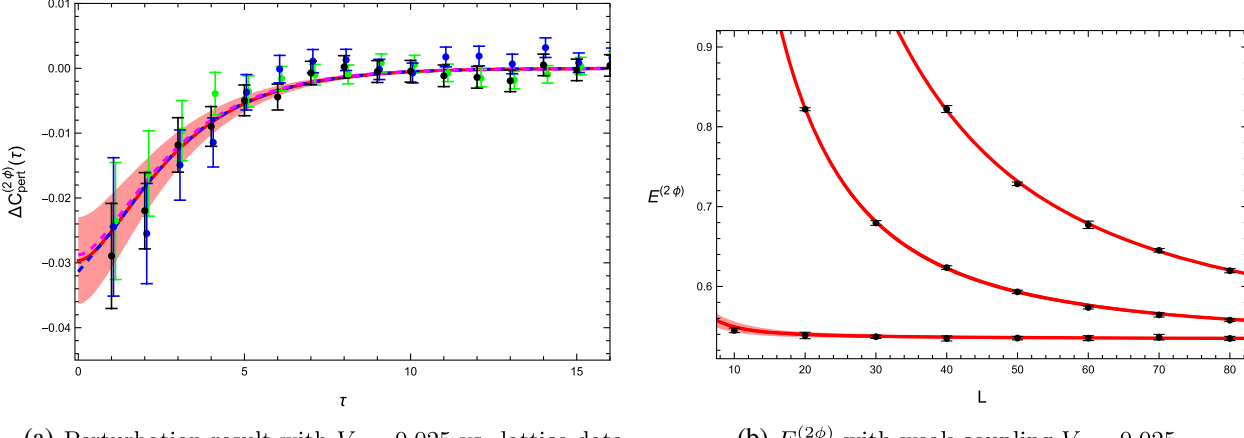
$$G_{2\phi}(p,\omega) = \frac{1}{T} \sum_{\omega' = \frac{2\pi n'}{L}}^{n' \in [0,T-1]} \frac{1}{2 - 2\cos\omega' - 2\cos k + 2\cosh m} \times \frac{1}{2 - 2\cos(\omega - \omega') - 2\cos k + 2\cosh m}.$$
(73)

At the limit of  $T \to \infty$  and zero lattice spacing,

$$G_{2\phi}(p,\omega) \xrightarrow[a\to 0]{T\to\infty} \frac{1}{\omega_p} \frac{1}{\omega^2 + (2\omega_p)^2}$$
 (74)

and

$$\Delta \tilde{C}_{\text{pert}}^{(2\phi)}(p,\tau) \overset{T \to \infty}{\underset{a \to 0}{\longrightarrow}} -V_0 \frac{\tau + \frac{1}{2\omega_p}}{(2\omega_p)^4} e^{-2\omega_p \tau}. \tag{75}$$



(a) Perturbation result with  $V_0 \sim 0.025$  vs. lattice data.

(b)  $E^{(2\phi)}$  with weak coupling  $V_0 \sim 0.025$ .

FIG. 7. (a) Comparison of the complete perturbation result of  $\triangle C_{\rm pert}^{(2\phi)}(\tau)$  given in Eq. (71) (dashed blue curves) vs approximation expression in Eq. (76) (red band) vs  $\triangle C^{(2\phi)}(\tau)$  by spectral representation in Eq. (69) (dashed purple curve) vs lattice data of L=30 (green error bars), 40 (blue error bars), and 50 (black error bars). (b) Comparison of two-particle energy spectra lattice data vs spectral generated by the Lüscher formula (red band) for weak coupling  $V_0 \sim 0.025$ . The model parameters are taken as  $\kappa=0.1235$ ,  $\lambda=0.001$ , T=120, and T=120

Hence, the perturbation result at the limit of zero lattice spacing in Eq. (39) is recovered. It can be shown numerically [see, e.g., Fig. 7(a)] that except at  $\tau = 0$ , Eq. (71) can be well approximated by

$$\Delta C_{\text{pert}}^{(2\phi)}(\tau) \simeq -\frac{V_0}{L} \sum_{p=\frac{2\pi n}{2}}^{n \in [-\frac{L}{2}+1,\frac{L}{2}]} \frac{\tau + \frac{1}{2\omega_p^{(a,L)}}}{(2\omega_p^{(a,L)})^3} e^{-2\omega_p^{(a,L)}\tau}.$$
(76)

The example of lattice data of  $\triangle C^{(2\phi)}(\tau)$  vs perturbation results is plotted in Fig. 7(a), as the comparison, the result of  $\triangle C^{(2\phi)}(\tau)$  by computing the spectral representation in

Eq. (69), is also shown in Fig. 7(a). With the same set of coupling strength,  $V_0 = 0.025 \pm 0.008$ , the low-lying two-particle spectra are computed by using the finite lattice spacing version quantization condition in Eq. (67) compared with lattice data [see Fig. 7(b)]. Overall, the consistency is excellent.

#### 2. Heavy $\phi$ field check

Next we also increase the mass of the  $\phi$  field by setting lattice model parameters to  $\kappa=0.122$  and  $\lambda=0.01$ . The single-particle mass and coupling strength in this case are about  $m=0.500\pm0.001$  and  $V_0=0.271\pm0.030$ , respectively.

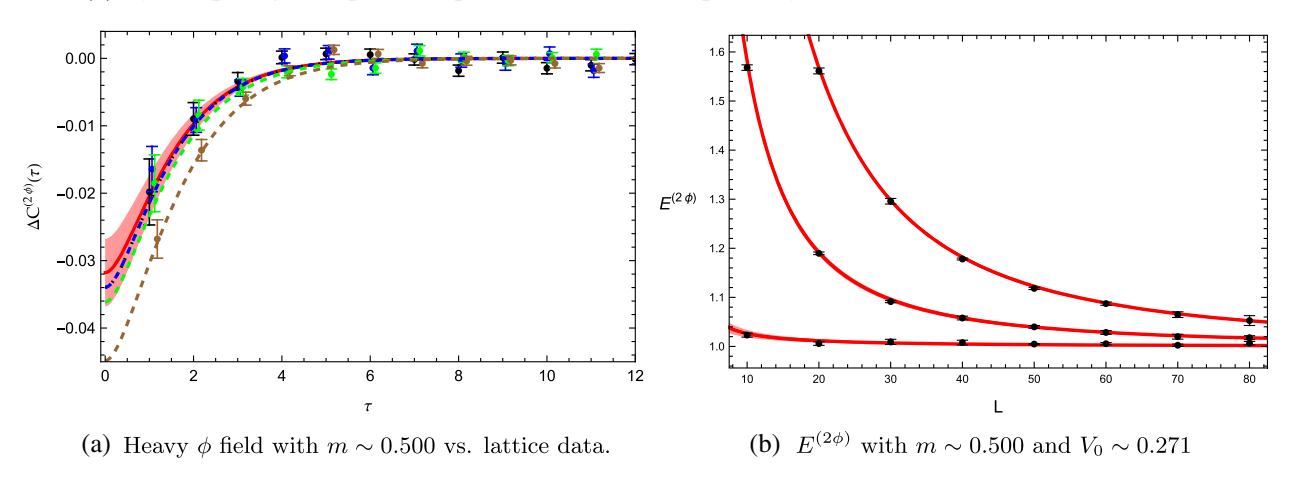


FIG. 8. (a) Comparison of the heavy  $\phi$  field infinite volume limit of  $\triangle C^{(2\phi)}(\tau)$  (solid red band) vs the spectral representation of  $\triangle C^{(2\phi)}(\tau)$  in Eq. (69) (dashed colored curves) vs lattice data of L=6 (brown error bars), L=10 (green error bars), 20 (blue error bars), and 30 (black error bars). (b) Comparison of two-particle energy spectra lattice data vs spectral generated by the Lüscher formula (red dashed curve) for the heavy  $\phi$  particle and coupling  $V_0 \sim 0.271$ . The model parameters are taken as  $\kappa = 0.122$ ,  $\lambda = 0.01$ , T=120, and T

The lattice data of  $\triangle C^{(2\phi)}(\tau)$  vs its infinite volume limit results are plotted in Fig. 8(a), and the result of  $\triangle C^{(2\phi)}(\tau)$  by computing the spectral representation in Eq. (69) is also shown in Fig. 8(a). With the same set of coupling strength,  $V_0=0.271\pm0.030$ , the low-lying two-particle spectra are computed by using the finite lattice spacing version quantization condition in Eq. (67) compared with lattice data [see Fig. 8(b)]. Again, both approaches show excellent consistency.

#### IV. SUMMARY AND DISCUSSION

In summary, a relativistic formalism that connects the difference of interacting and noninteracting two-particle correlation functions to the scattering phase shift by an integral is derived, and the main result is shown in Eq. (3). The difference of finite volume two-particle correlation functions converges rapidly to its infinite volume limit near small Euclidean times as the size of the finite box is increased. Hence, the proposed approach may have a good potential to overcome the S/N problem in the lattice calculation of two-nucleon interactions.

The numerical tests are conducted by (1) analytic solutions of an exactly solvable contact interaction model, (2) perturbation calculation, and (3) Monte Carlo simulation of the  $\phi^4$  lattice field theory model.

In Monte Carlo simulation of the  $\phi^4$  theory, the model with four different sets of parameters is calculated, and the single-particle mass and coupling strength are extracted accordingly (see Table I). The first set  $(\kappa, \lambda) = (0.1213, 0)$ represents noninteracting  $\phi$  fields, and it is used to check the lattice dispersion relation, as well as agreements of analytic expressions of noninteracting correlation functions vs lattice data. The second set  $(\kappa, \lambda) = (0.1286, 0.01)$ represents interacting particles with a mass of  $m \sim 0.272$ and a coupling strength of  $V_0 \sim 0.20$  (our approach) or  $V_0 \sim 0.17$  (Lüscher formula approach). The coupling strengths extracted from two different approaches differ slightly within errors. The difference may be caused by an inelastic channel contribution: the Lüscher formula approach fits only low-lying energy spectra, but the integrated correlation function approach fits the sum of all energy levels and may be considered as a "global fit"

TABLE I. List of sets of  $\phi^4$  model parameters  $(\kappa, \lambda)$ , and corresponding single-particle mass and coupling strength  $V_0$ .

$(\kappa,\lambda)$	m	$V_0$
(0.1213, 0)	$0.350 \pm 0.003$	0
(0.1286, 0.01)	$0.272 \pm 0.003$	$0.20 \pm 0.03$ vs $0.17 \pm 0.04$
(0.1235, 0.001)	$0.267 \pm 0.003$	$0.025 \pm 0.008$
(0.1220, 0.01)	$0.500 \pm 0.001$	$0.27 \pm 0.03$

approach. The inelastic contributions are not yet included in our formalism at the current scope, which may show at a small Euclidean time region. At the current  $\phi^4$  lattice model, there are no three-to-two particles coupling, so the inelastic threshold starts at  $4m \sim 1.1$ , and the inelastic effects are not significantly suppressed by  $\frac{e^{-E_n\tau}}{E_n}$  near  $\tau \sim 0$ . As a sanity check, two other sets of parameters are chosen to simulate scenarios of (1) weak coupling strength  $V_0 \sim$ 0.025 with  $m \sim 0.267$ , and (2) heavy mass  $m \sim 0.5$  with  $V_0 \sim 0.27$ . The inelastic contributions are suppressed in both scenarios: (1) four-particle interaction shows up at an order of  $V_0^2$  in a weak coupling scenario, and (2) the  $4\phi$ threshold starts now at  $4m \sim 2$  in a heavy mass scenario. Numerically, both scenarios show good agreement between the proposed approach and the Lüscher formula approach. On the other hand, the inelastic effect and coupled-channel dynamics should be installed and studied in a more rigorous way, which will be carried out in our further publications.

At last, we comment that both the Lüscher formula approach and the integrated correlation function approach proposed in this manuscript have their own pros and cons. The Lüscher formula offers a model-independent way of extracting elastic scattering phase shifts, which convert one energy level from the lattice calculation into one point of phase shift directly. However, it suffers difficulties at a large volume calculation or S/N problem. On the other hand, the integrated correlation function approach in principle is also a model independent approach [see, e.g., Eq. (3)]. However, the difference of the integrated correlation function is related to the phase shift by an integral, and hence, the phase shift cannot be pulled out from lattice data point-by-point directly. Instead, we have to first model and parametrize the scattering phase shift in terms of a few parameters and kinematic factors based on either the chiral perturbation theory or the K-matrix formalism. The phase shift can then be obtained by fitting lattice data of integrated correlation functions with these free parameters through an integral. The advantage of the integrated correlation function approach is that it shows the rapid convergence as the volume is increased, and it also shows potentials to overcome the S/N problem, which may be useful in the nucleon-nucleon interaction lattice calculation.

#### ACKNOWLEDGMENTS

We acknowledge support from the College of Arts and Sciences and Faculty Research Initiative Program, Dakota State University, Madison, SD. P. G. acknowledges computing resources (https://cloud.madren.org/) at DSU made available for conducting the research reported in this work. This research was supported in part by the National Science Foundation under Grant No. NSF PHY-1748958.

# APPENDIX A: RELATIVISTIC TWO-PARTICLE SCATTERING SOLUTIONS IN INFINITE VOLUME

## 1. Relativistic Lippmann-Schwinger-like equation and scattering amplitude

For the short-range interaction, the scattering of relativistic particles may be well described by relativistic Lippmann-Schwinger-like equation (see, e.g., Refs. [17,39]), where the relativistic Lippmann-Schwinger-like equations can be derived from Bethe-Salpeter equations with an assumption of the "instantaneous interaction kernel" [17,39].

In the present work, a contact interaction is considered,

$$V(r) = V_0 \delta(r);$$

hence, only even parity states are affected by interaction. The scattering solutions can be found in Appendix B in Ref. [17]. The relative scattering wave function satisfies LS-like equation

$$\psi_{E_k}^{(\infty)}(r) = \cos(kr) + G_0^{(\infty)}(r, E_k) V_0 \psi_{E_k}^{(\infty)}(0), \quad (A1)$$

where  $k = \sqrt{\frac{E_k^2}{4} - m^2}$  is the relative momentum of two particles in the CM frame and free particles of Green's function are defined by

$$G_0^{(\infty)}(r;E) = \int_{-\infty}^{\infty} \frac{dq}{2\pi} \frac{1}{\sqrt{q^2 + m^2}} \frac{e^{iqr}}{E^2 - 4(q^2 + m^2) + i0}.$$
(A2)

The scattering amplitude is introduced by

$$t(E) = -\frac{1}{\frac{1}{V_0} - G_0^{(\infty)}(0; E)},$$
 (A3)

and hence, the wave function can be rewritten as

$$\psi_{E_k}^{(\infty)}(r) = \cos(kr) - t(E_k)G_0^{(\infty)}(r, E_k).$$
 (A4)

The function  $G_0^{(\infty)}(0; E)$  is an analytic function of  $E^2$  with a branch cut starting at threshold  $4m^2$ ,

$$G_0^{(\infty)}(0;E) = \frac{1}{2\pi} \int_{4m^2}^{\infty} ds' \frac{1}{\sqrt{s'(s'-4m^2)}} \frac{1}{E^2 - s' + i0}.$$
(A5)

The analytic expression of  $G_0^{(\infty)}(0;E)$  can be found rather straightforwardly,

$$G_0^{(\infty)}(0;E) = \frac{\rho(E)}{\pi} \left[ \ln \frac{E^2 - 2m^2 + \sqrt{E^2(E^2 - 4m^2)}}{2m^2} - i\pi\theta(E - 2m) \right],\tag{A6}$$

where

$$\rho(E) = \frac{1}{2} \frac{1}{\sqrt{E^2(E^2 - 4m^2)}}.$$
 (A7)

The scattering amplitude can be parametrized by a phase shift,

$$t(E) = \frac{1}{\rho(E)} \frac{e^{2i\delta(E)} - 1}{2i} = \frac{1}{\rho(E)} \frac{1}{\cot \delta(E) - i},$$
 (A8)

and the on-shell unitarity relation is determined by

$$\operatorname{Im}[t^{-1}(E)] = -\theta(E - 2m)\rho(E). \tag{A9}$$

The scattering amplitude can also be expressed in terms of the Muskhelishvili-Omnès (MO) representation [60,61] that is sometimes also referred to as the N/D method [62,63] (also see, e.g., Refs. [64–69]),

$$t(E) = Ne^{\frac{1}{\pi} \int_{4m^2}^{\infty} ds \frac{\delta(\sqrt{s})}{s - E^2 - i0}},$$
 (A10)

where  $N = t(2m)e^{-\frac{1}{\pi}\int_{4m^2}^{\infty} ds \frac{\delta(\sqrt{s})}{s-4m^2-i0}}$  is a constant factor.

# 2. Two-particle Green's function and its spectral representation

Relativistic two-particle Green's function may be introduced by Dyson equation

$$\begin{split} G^{(\infty)}(r,r';E) \\ &= G_0^{(\infty)}(r-r';E) + G_0^{(\infty)}(r;E) V_0 G^{(\infty)}(0,r';E), \quad \text{(A11)} \end{split}$$

and the analytic solution is thus given by

$$G^{(\infty)}(r, r'; E) - G_0^{(\infty)}(r - r'; E)$$

$$= -G_0^{(\infty)}(r; E)t(E)G_0^{(\infty)}(r'; E). \tag{A12}$$

Spectral representation of Green's function is given by

$$G^{(\infty)}(r,r';E) = \int_{-\infty}^{\infty} \frac{dq}{2\pi} \frac{1}{\sqrt{q^2 + m^2}} \frac{\psi_{E_q}^{(\infty)}(r)\psi_{E_q}^{(\infty)*}(r') + \sin(qr)\sin(qr')}{E^2 - E_q^2 + i0},$$
(A13)

where  $E_q = 2\sqrt{q^2 + m^2}$ . The  $\sin(qr)$  is the wave function of odd parity states that will be canceled out between interacting and noninteracting Green's function and do not contribute on the right-hand side of Eq. (A12).

## 3. Integrated Green's function and its relation to the scattering phase shift

Using Eq. (A12) and the analytic expression of free particles Green's function in Eq. (A2), we find

$$\tilde{G}^{(\infty)}(p,p;E) - \tilde{G}_0^{(\infty)}(p-p;E) = \frac{1}{\sqrt{p^2 + m^2}} t(E) \frac{d}{dE^2} \left[ \frac{1}{\sqrt{p^2 + m^2}} \frac{1}{E^2 - E_p^2 + i0} \right], \quad (A14)$$

where the momentum space Green's function is defined by

$$\tilde{G}^{(\infty)}(p,p';E) = \int_{-\infty}^{\infty} dr dr' e^{ipr} G^{(\infty)}(r,r';E) e^{-ip'r'}. \quad (A15)$$

Hence, the difference of integrated Green's functions is given in terms of the scattering amplitude by

$$\begin{split} & \int_{-\infty}^{\infty} \frac{dp}{2\pi} \sqrt{p^2 + m^2} [\tilde{G}^{(\infty)}(p, p; E) - \tilde{G}_0^{(\infty)}(p - p; E)] \\ & = \frac{d}{dE^2} \ln[t(E)]. \end{split} \tag{A16}$$

Using the MO representation of the scattering amplitude in Eq. (A10), thus we finally find

$$\int_{-\infty}^{\infty} \frac{dp}{2\pi} \sqrt{p^2 + m^2} [\tilde{G}^{(\infty)}(p, p; E) - \tilde{G}_0^{(\infty)}(p - p; E)]$$

$$= -\frac{1}{\pi} \int_{4m^2}^{\infty} ds \frac{\delta(\sqrt{s})}{(s - E^2 - i0)^2}.$$
(A17)

The imaginary part of Eq. (A17) yields

$$\begin{split} &\int_{-\infty}^{\infty} \frac{dp}{2\pi} \frac{1}{2\omega_p} \left[ \tilde{\psi}_{E_k}^{(\infty)}(p) \tilde{\psi}_{E_k}^{(\infty)*}(p) - \tilde{\psi}_{E_k}^{(0,\infty)}(p) \tilde{\psi}_{E_k}^{(0,\infty)*}(p) \right] \\ &= -4k \frac{d}{dE_k} \delta(E_k), \end{split} \tag{A18}$$

where

$$\tilde{\psi}_{E_k}^{(0,\infty)}(p) = 2\omega_p \frac{\delta_{k,p} + \delta_{k,-p}}{2}.$$
 (A19)

Equation (A18) may be considered as the normalization of the scattering wave function, and the finite term on the right-hand side of the equation is the result of the boundary condition of scattering solutions (see discussion in Ref. [70]). As the matter of fact, when condition

$$\int_{-\infty}^{\infty} \frac{dp}{2\pi} \frac{1}{2\omega_p} \tilde{\psi}_E^{(\infty)}(p) \tilde{\psi}_{E'}^{(\infty)*}(p) = 0 \quad \text{for } E \neq E'$$
 (A20)

is imposed, the on-shell unitarity relation of the scattering amplitude in Eq. (A9) can be further generalized to

$$t(E) - t^*(E') = [G_0^{(\infty)}(0; E) - G_0^{(\infty)*}(0; E')]t^*(E')t(E).$$
(A21)

## APPENDIX B: RELATIVISTIC LIPPMANN-SCHWINGER-LIKE EQUATION IN FINITE VOLUME AND RANDOM PHASE APPROXIMATION

In this section, we show that the relativistic Lippmann-Schwinger-like equations can be derived from random phase approximation (RPA) [71]. The Hamiltonian of the lattice field theory defined in Eq. (4) is given by the free particles term

$$\hat{H}_0 = \frac{1}{L} \sum_{p=\frac{2\pi n}{2}}^{n \in \mathbb{Z}} \omega_p(\hat{a}_p^{\dagger} \hat{a}_p + \hat{b}_p^{\dagger} \hat{b}_p), \tag{B1}$$

and the interaction term

$$\hat{H}_I = \frac{1}{4!} \int_0^L dx dy |\hat{\phi}(x)|^2 V(x - y) |\hat{\phi}(y)|^2, \quad (B2)$$

where

$$\hat{\phi}(x) = \frac{1}{L} \sum_{p=\frac{2\pi n}{2}}^{n \in \mathbb{Z}} \frac{1}{\sqrt{2\omega_p}} \left[ e^{ipx} \hat{a}_p^{\dagger} + e^{-ipx} \hat{b}_p \right], \quad (B3)$$

where  $\omega_p = \sqrt{p^2 + m^2}$ . The  $\hat{a}_p^{\dagger}(\hat{a}_p)$  and  $\hat{b}_p^{\dagger}(\hat{b}_p)$  are creation (annihilation) operators of particles and antiparticles, respectively, and they satisfy commutation relations,

$$[\hat{a}_{p}, \hat{a}_{p'}^{\dagger}] = [\hat{b}_{p}, \hat{b}_{p'}^{\dagger}] = L\delta_{p,p'}.$$
 (B4)

Based on the RPA assumption, the two-particle states can be created by creating two particles from vacuum or equivalently by annihilating two antiparticles in the vacuum, so the two-particle wave function is defined by

$$\tilde{\psi}_E^{(a)}(p) = \langle E | \frac{1}{\sqrt{2}} \hat{a}_p^{\dagger} \hat{a}_{-p}^{\dagger} | 0 \rangle \tag{B5}$$

and

$$\tilde{\psi}_E^{(b)}(p) = \langle E | \frac{1}{\sqrt{2}} \hat{b}_p \hat{b}_{-p} | 0 \rangle, \tag{B6}$$

where superscripts (a) and (b) are used to label the two-particle wave functions created by two different mechanisms.

The dynamical equations of two-particle states under RPA are derived from

$$\langle E | \left[ \hat{H}, \frac{1}{\sqrt{2}} \hat{a}_p^{\dagger} \hat{a}_{-p}^{\dagger} \right] | 0 \rangle = E \tilde{\psi}_E^{(a)}(p)$$
 (B7)

and

$$\langle E|\left[\hat{H}, \frac{1}{\sqrt{2}}\hat{b}_p\hat{b}_{-p}\right]|0\rangle = E\tilde{\psi}_E^{(b)}(p),$$
 (B8)

where  $\hat{H} = \hat{H}_0 + \hat{H}_I$  is the full Hamiltonian operator. After some length calculations, we finally find coupled equations,

$$\tilde{\psi}_{E}^{(a)}(p) = \frac{1}{2\omega_{p}} \frac{1}{E - 2\omega_{p}} \times \frac{1}{L} \sum_{p' = \frac{2\pi n'}{L}}^{n' \in \mathbb{Z}} \frac{1}{2\omega_{p'}} \tilde{V}(p - p') [\tilde{\psi}_{E}^{(a)}(p') + \tilde{\psi}_{E}^{(b)}(p')]$$
(B9)

and

$$\begin{split} \tilde{\psi}_E^{(b)}(p) &= -\frac{1}{2\omega_p} \frac{1}{E + 2\omega_p} \\ &\times \frac{1}{L} \sum_{p' = \frac{2\pi n'}{L}}^{n' \in \mathbb{Z}} \frac{1}{2\omega_{p'}} \tilde{V}(p - p') \big[ \tilde{\psi}_E^{(a)}(p') + \tilde{\psi}_E^{(b)}(p') \big], \end{split}$$

where  $\tilde{V}(p) = \int_0^L dr e^{ipr} V(r)$  is the Fourier transform of the interaction potential. Two equations can be combined together by defining

$$\tilde{\psi}_E(p) = \tilde{\psi}_E^{(a)}(p) + \tilde{\psi}_E^{(b)}(p),$$
 (B11)

and we thus find

$$\frac{\tilde{\psi}_{E}(p)}{2\omega_{p}} = \frac{1}{\omega_{p}} \frac{1}{E^{2} - (2\omega_{p})^{2}} \frac{1}{L} \sum_{p' = \frac{2\pi n'}{2}}^{n' \in \mathbb{Z}} \tilde{V}(p - p') \frac{\tilde{\psi}_{E}(p')}{2\omega_{p'}}.$$
 (B12)

Next let us define the coordinate space wave function by

$$\psi_E^{(L)}(r) = \frac{1}{L} \sum_{p=\frac{2\pi n}{L}}^{n \in \mathbb{Z}} e^{-ipr} \frac{\tilde{\psi}_E(p)}{2\omega_p}, \quad (B13)$$

and we thus find

$$\psi_E^{(L)}(r) = \int_0^L dr \left[ \frac{1}{L} \sum_{p = \frac{2\pi n}{L}}^{n \in \mathbb{Z}} \frac{1}{\omega_p} \frac{e^{ip(r-r')}}{E^2 - (2\omega_p)^2} \right] V(r') \psi_E^{(L)}(r'),$$
(B14)

which is consistent with the result that is derived from Bethe-Salpeter equations with an assumption of the "instantaneous interaction kernel" [17,39].

(B10)

<sup>[1]</sup> K. Hebeler, J. Holt, J. Menéndez, and A. Schwenk, Annu. Rev. Nucl. Part. Sci. 65, 457 (2015).

<sup>[2]</sup> P. Navrátil, S. Quaglioni, G. Hupin, C. Romero-Redondo, and A. Calci, Phys. Scr. **91**, 053002 (2016).

<sup>[3]</sup> J. Engel and J. Menéndez, Rep. Prog. Phys. 80, 046301 (2017).

<sup>[4]</sup> M. Lüscher, Nucl. Phys. **B354**, 531 (1991).

<sup>[5]</sup> S. Aoki *et al.* (CP-PACS Collaboration), Phys. Rev. D 76, 094506 (2007).

<sup>[6]</sup> X. Feng, K. Jansen, and D. B. Renner, Phys. Rev. D 83, 094505 (2011).

<sup>[7]</sup> C. B. Lang, D. Mohler, S. Prelovsek, and M. Vidmar, Phys. Rev. D 84, 054503 (2011); 89, 059903(E) (2014).

<sup>[8]</sup> S. Aoki *et al.* (CS Collaboration), Phys. Rev. D **84**, 094505 (2011).

<sup>[9]</sup> J. J. Dudek, R. G. Edwards, and C. E. Thomas, Phys. Rev. D 86, 034031 (2012).

<sup>[10]</sup> J. J. Dudek, R. G. Edwards, and C. E. Thomas (Hadron Spectrum Collaboration), Phys. Rev. D 87, 034505 (2013); 90, 099902(E) (2014).

<sup>[11]</sup> D. J. Wilson, J. J. Dudek, R. G. Edwards, and C. E. Thomas, Phys. Rev. D 91, 054008 (2015).

<sup>[12]</sup> D. J. Wilson, R. A. Briceño, J. J. Dudek, R. G. Edwards, and C. E. Thomas, Phys. Rev. D 92, 094502 (2015).

<sup>[13]</sup> J. J. Dudek, R. G. Edwards, and D. J. Wilson (Hadron Spectrum Collaboration), Phys. Rev. D 93, 094506 (2016).

<sup>[14]</sup> S. R. Beane, W. Detmold, T. C. Luu, K. Orginos, M. J. Savage, and A. Torok, Phys. Rev. Lett. 100, 082004 (2008).

- [15] W. Detmold, M. J. Savage, A. Torok, S. R. Beane, T. C. Luu, K. Orginos, and A. Parreno, Phys. Rev. D 78, 014507 (2008).
- [16] B. Hörz and A. Hanlon, Phys. Rev. Lett. **123**, 142002 (2019).
- [17] P. Guo and B. Long, Phys. Rev. D 101, 094510 (2020).
- [18] K. Rummukainen and S. A. Gottlieb, Nucl. Phys. **B450**, 397 (1995).
- [19] N. H. Christ, C. Kim, and T. Yamazaki, Phys. Rev. D 72, 114506 (2005).
- [20] V. Bernard, M. Lage, U.-G. Meißner, and A. Rusetsky, J. High Energy Phys. 08 (2008) 024.
- [21] S. He, X. Feng, and C. Liu, J. High Energy Phys. 07 (2005) 011.
- [22] M. Lage, U.-G. Meißner, and A. Rusetsky, Phys. Lett. B 681, 439 (2009).
- [23] M. Döring, U.-G. Meißner, E. Oset, and A. Rusetsky, Eur. Phys. J. A 47, 139 (2011).
- [24] P. Guo, J. Dudek, R. Edwards, and A. P. Szczepaniak, Phys. Rev. D 88, 014501 (2013).
- [25] P. Guo, Phys. Rev. D 88, 014507 (2013).
- [26] S. Kreuzer and H. W. Hammer, Phys. Lett. B 673, 260 (2009).
- [27] K. Polejaeva and A. Rusetsky, Eur. Phys. J. A 48, 67 (2012).
- [28] M. T. Hansen and S. R. Sharpe, Phys. Rev. D 90, 116003 (2014).
- [29] M. Mai and M. Döring, Eur. Phys. J. A 53, 240 (2017).
- [30] M. Mai and M. Döring, Phys. Rev. Lett. **122**, 062503 (2019).
- [31] M. Döring, H. W. Hammer, M. Mai, J. Y. Pang, A. Rusetsky, and J. Wu, Phys. Rev. D 97, 114508 (2018).
- [32] P. Guo, Phys. Rev. D 95, 054508 (2017).
- [33] P. Guo and V. Gasparian, Phys. Lett. B 774, 441 (2017).
- [34] P. Guo and V. Gasparian, Phys. Rev. D 97, 014504 (2018).
- [35] P. Guo and T. Morris, Phys. Rev. D 99, 014501 (2019).
- [36] M. Mai, M. Döring, C. Culver, and A. Alexandru, Phys. Rev. D 101, 054510 (2020).
- [37] P. Guo, M. Döring, and A. P. Szczepaniak, Phys. Rev. D 98, 094502 (2018).
- [38] P. Guo, Phys. Lett. B 804, 135370 (2020).
- [39] P. Guo and M. Döring, Phys. Rev. D 101, 034501 (2020).
- [40] P. Guo, Phys. Rev. D 101, 054512 (2020).
- [41] P. Guo, arXiv:2007.04473.
- [42] P. Guo and B. Long, Phys. Rev. D 102, 074508 (2020).
- [43] P. Guo, Phys. Rev. D 102, 054514 (2020).
- [44] P. Guo and V. Gasparian, Phys. Rev. D 103, 094520 (2021).
- [45] P. Guo and B. Long, J. Phys. G 49, 055104 (2022).

- [46] P. Guo, Phys. Rev. C 103, 064611 (2021).
- [47] P. Guo and V. Gasparian, J. Phys. A 55, 265201 (2022).
- [48] G. P. Lepage, Boulder ASI 1989, 97 (1989).
- [49] C. Drischler, W. Haxton, K. McElvain, E. Mereghetti, A. Nicholson, P. Vranas, and A. Walker-Loud, Prog. Part. Nucl. Phys. 121, 103888 (2021).
- [50] J. Bulava and M. T. Hansen, Phys. Rev. D 100, 034521 (2019).
- [51] N. Ishii, S. Aoki, and T. Hatsuda, Phys. Rev. Lett. 99, 022001 (2007).
- [52] S. Aoki, T. Hatsuda, and N. Ishii, Prog. Theor. Phys. 123, 89 (2010).
- [53] T. Iritani, S. Aoki, T. Doi, S. Gongyo, T. Hatsuda, Y. Ikeda, T. Inoue, N. Ishii, H. Nemura, and K. Sasaki (HAL QCD Collaboration), Phys. Rev. D 99, 014514 (2019).
- [54] N. Ishii, S. Aoki, T. Doi, T. Hatsuda, Y. Ikeda, T. Inoue, K. Murano, H. Nemura, and K. Sasaki, Phys. Lett. B 712, 437 (2012).
- [55] S. Aoki, Eur. Phys. J. A 49, 81 (2013).
- [56] M. Hansen, A. Lupo, and N. Tantalo, Phys. Rev. D 99, 094508 (2019).
- [57] G. Bailas, S. Hashimoto, and T. Ishikawa, Prog. Theor. Exp. Phys. 2020, 043B07 (2020).
- [58] P. Guo and V. Gasparian, preceding paper Phys. Rev. D 108, 074504 (2023).
- [59] M. Luscher and U. Wolff, Nucl. Phys. **B339**, 222 (1990).
- [60] N. Muskhelishvili, Trans. Inst. Math. Tbilissi 10, 1 (1941).
- [61] R. Omnes, Nuovo Cimento 8, 316 (1958).
- [62] G. F. Chew and S. Mandelstam, Phys. Rev. **119**, 467 (1960).
- [63] G. Frye and R. L. Warnock, Phys. Rev. 130, 478 (1963).
- [64] M. Gorchtein, P. Guo, and A. P. Szczepaniak, Phys. Rev. C 86, 015205 (2012).
- [65] I. V. Danilkin, C. Fernández-Ramírez, P. Guo, V. Mathieu, D. Schott, M. Shi, and A. P. Szczepaniak, Phys. Rev. D 91, 094029 (2015).
- [66] P. Guo, I. V. Danilkin, and A. P. Szczepaniak, Eur. Phys. J. A 51, 135 (2015).
- [67] P. Guo, I. V. Danilkin, D. Schott, C. Fernández-Ramírez, V. Mathieu, and A. P. Szczepaniak, Phys. Rev. D 92, 054016 (2015).
- [68] P. Guo, I. V. Danilkin, C. Fernández-Ramírez, V. Mathieu, and A. P. Szczepaniak, Phys. Lett. B **771**, 497 (2017).
- [69] P. Guo and V. Gasparian, Phys. Rev. Res. 4, 023083 (2022).
- [70] N. Poliatzky, Helv. Phys. Acta 66, 241 (1993).
- [71] A. L. Fetter and J. D. Walecka, *Quantum Theory of Many-Particle Systems* (McGraw-Hill, Boston, 1971).